Characterization of aerosol number size distributions and their effect on cloud properties at Syowa Station, Antarctica

Keiichiro Hara[1], Chiharu Nishita-Hara[2], Kazuo Osada[3], Masanori Yabuki[4], and Takashi Yamanouchi[5]

[1] Department of Earth System Science, Faculty of Science, Fukuoka University, Fukuoka, 814-0180, Japan
5 [2] Fukuoka Institute for Atmospheric Environment and Health, Fukuoka University, Fukuoka, 814-0180, Japan
[3] Graduate School of Environmental Studies, Nagoya University, Nagoya, 464-8601, Japan
[4] Research Institute for Sustainable Humanosphere, Kyoto University, Kyoto, 611-0011, Japan
[5] National Institute of Polar Research, Tokyo, 190-0014, Japan

10 *Correspondence to*: Keiichiro Hara (harakei@fukuoka-u.ac.jp)

Abstract. We took aerosol measurements at Syowa Station, Antarctica to characterize the aerosol number–size distribution and other aerosol physicochemical properties in 2004 – 2006. Four modal structures (i.e., mono-, bi-, tri-, and quad-modal) were identified in aerosol size distributions during measurements. Particularly, tri- and quad-modal structures were associated closely with new particle formation (NPF). To elucidate where NPF proceeds in the Antarctic, we compared the aerosol size distributions and modal structure to air mass origins computed using backward trajectory analysis. Results of this comparison imply that aerosol size distributions involved with fresh NPF (quad-modal distributions) were observed in coastal and continental free troposphere (12 % of days) and marine and coastal boundary layer (1 %) during September – October and March, and in coastal and continental free troposphere (3 %) and marine and coastal boundary layer (8 %) during December – February. Photochemical gaseous products, coupled with UV radiation, play an important role in NPF, even in the Antarctic troposphere. With the appearance of the ozone hole in the Antarctic stratosphere, more UV radiation can enhance atmospheric chemistry, even near the surface in the Antarctic. However, linkage among tropospheric aerosols in the Antarctic, ozone hole, and UV enhancement is unknown. Results demonstrated that NPF started in the Antarctic free troposphere already in the end-August – early September by UV enhancement resulting from the ozone hole. Then, aerosol particles supplied from NPF during the periods with appearance of ozone hole grow gradually by vapor condensation, suggesting modification of aerosol properties such as number concentrations and size distributions in the Antarctic troposphere during summer. Here, we assess the hypothesis that UV enhancement in the upper troposphere by the Antarctic ozone hole modifies the aerosol population, aerosol size distribution, cloud condensation nuclei capabilities, and cloud properties in Antarctic regions during summer.

1 Introduction

The Antarctic is isolated from human activities occurring in the mid-latitudes. In spite of the slight amount of human activity
30 in the Antarctic, such as research activities at each station and tourism mostly in the Antarctic Peninsula during summer, the source strength of anthropogenic species (e.g., black carbon from combustion processes) is negligible in the Antarctic circle at the moment (e.g., Weller et al., 2013; Hara et al., 2019). Consequently, aerosol measurements in the Antarctic have been taken to ascertain aerosol physicochemical properties, atmospheric chemistry, and their effects on climate change in Earth's background conditions (i.e., cleanest and pristine conditions).

35

Despite the cleanest conditions prevailing in the Antarctic, concentrations of condensation nuclei (CN) show clear seasonal variations with maximum in summer and minimum in winter (Gras et al., 1993; Hara et al., 2011a; Weller et al., 2011). This seasonal variation relates to supply and deposition processes. In addition to primary aerosol emissions such as sea-salt aerosols from sea-surface and sea-ice regions (e.g., Hara et al., 2020), atmospheric aerosol formation (i.e. new particle formation, NPF)

1

40   is important to supply atmospheric aerosols (Kulmala et al., 2013; Kerminen et al., 2018) and to affect climate through indirect processes (Asmi et al., 2010; Dall'Osto et al., 2017). Continuous measurements of aerosol size distributions were carried out to understand and discuss (1) NPF, (2) particle growth, (3) volatility as indirect information of aerosol constituents, and (4) hygroscopicity and ability of cloud condensation nuclei (CCN) using scanning mobility particle sizer (SMPS) in the Antarctic (Koponen et al., 2003; Virkkula et al., 2007; Asmi et al., 2010; Hara et al., 2011b; Kyrö et al., 2013; Järvinen et al., 2013;

45   Weller et al., 2015; Jokinen et al., 2018; Kim et al., 2019; Jang et al., 2019; Lachlan-Cope et al., 2020) and similar instrument (Ito, 1993). Seasonal features of aerosol number concentrations are associated with primary emission of sea-salt aerosols, NPF, emissions of aerosol precursors from oceanic bioactivity, and photochemical processes (e.g., Koponen et al., 2003; Virkkula et al., 2007; Asmi et al., 2010; Hara et al., 2011a, 2011b, 2020; Kyrö et al., 2013; Järvinen et al., 2013; Fiebig et al., 2014; Weller et al., 2015; Humphries et al., 2016; Jang et al., 2019; Frey et al., 2020). Aerosol volatility measurements presented

50   high abundance of less-volatile particles due to dominance of sea-salt particles even in ultrafine mode (smaller than 100 nm in diameter) during winter – early spring, whereas volatile particles such as H_2SO_4 and organics were dominant during spring – summer (Asmi et al., 2010; Hara et al., 2011b; Weller et al., 2011). In polar regions during winter – early spring, sea-salt particles in ultrafine – coarse modes were released from snow and sea-ice surfaces via wind blowing and sublimation (e.g., Hara et al., 2012, 2017, 2020; Frey et al., 2020). In addition to primary emission of sea-salt aerosols in colder seasons, NPF

55   was observed along the Antarctic coasts during summer at the boundary layer (Koponen et al., 2003; Virkkula et al., 2007; Asmi et al., 2010; Kyrö et al., 2013; Weller et al., 2015; Jokinen et al., 2018; Kim et al., 2019; Jang et al., 2019; Lachlan-Cope et al., 2020) and in the free troposphere (Hara et al., 2011a; Humphries et al., 2016; Lachlan-Cope et al., 2020). Particularly, NPF events at Neumayer, Aboa, and King Sejong during summer were observed in the air masses transported from marine boundary layer with no or less sea ice density (Weller et al., 2015; Jokinen et al., 2018; Kim et al., 2019). In addition to NPF

60   in marine boundary layer, NPF and high CN concentrations were identified in free troposphere and the air masses transported from free troposphere (Hara et al., 2011a; Humphries et al., 2016; Lachlan-Cope et al., 2020). Moreover, NPF occurred around melt-ponds on the Antarctic continent during summer (Kyrö et al., 2013). Although most earlier works have specifically examined summer NPF in the Antarctic (Koponen et al., 2003; Virkkula et al., 2007; Asmi et al., 2010; Kyrö et al., 2013; Weller et al., 2015; Jokinen et al., 2018), some investigations (Hara et al., 2011a; Järvinen et al., 2013; Kim et al., 2019) have

65   emphasized that NPF occurs as early as September in the Antarctic.

Knowledge and discussion on condensable vapors (i.e., aerosol precursors) are essential to elucidate microphysical processes such as NPF and growth, and location where NPF occurs. Earlier works have emphasized examination of the following condensable vapors (i.e., aerosol precursors) for NPF and particle growth: H_2SO_4, CH_3SO_3H, HIO_3, NH_3, amines, and other

70   organics with low vapor pressure (Yu et al., 2012; Kulmala et al., 2013; Kyrö et al., 2013; Weller et al., 2015; Simplä et al., 2016; Jen et al., 2016; Jokinen et al., 2018; Shen et al., 2019; Burrell et al., 2019). Gaseous H_2SO_4 has been considered as one of the most important aerosol precursors (e.g., Kulmala et al., 2013; Kerminen et al., 2018). H_2SO_4 is converted via photochemical oxidation of dimethylesufide (DMS) and SO_2 dominantly released from biogenic activity in the ocean (e.g., Minikin et al., 1998; Weller et al., 2015; Enami et al., 2017; Jang et al., 2019). Indeed, high DMS concentrations in the

75   Antarctic were found in sea-ice margin and marine boundary layer during summer (Koga et al., 2014). The concentrations of H_2SO_4 and CH_3SO_3H showed diurnal change with maximum in daytime at Palmer station (Jefferson et al., 1998a, 1998b). Also, NPF often occurred in daytime at Neumayer and Aboa during summer (Asmi et al., 2010; Weller et al., 2015; Jokinen et al., 2018). Measurement of aerosol hygroscopicity at Aboa indicated an important role of organic vapors for the growth of freshly nucleated particles (Asmi et al., 2010). Recently, simultaneous measurements of aerosol precursors and aerosol size

80   distributions exhibited that H_2SO_4 and NH_3 had significant contribution to NPF and growth at Aboa in the air masses from marine boundary layer (Jokinen et al., 2018). Condensable vapors other than H_2SO_4 and NH_3, for example iodine compounds

such as HIO$_3$ and organics, are associated with atmospheric and snowpack chemistry (e.g., Saiz-Lopez et al., 2008; Atkinson et al., 2012; Roscoe et al., 2015; Simplä et al., 2016; Hara et al., 2020), and oceanic bioactivity (Dall'Osto et al., 2019). Contribution of the condensable vapors to NPF and growth has been discussed and unclear in the Antarctic.

85

Some condensable vapors for NPF and growth are formed through photochemical reactions with atmospheric oxidants such as OH, O$_3$, and BrO (Read et al., 2008). They relate to UV radiation (Matsumi et al., 2002; Matsumi and Kawasaki, 2003). Appearance of the ozone hole in the Antarctic stratosphere during September–November (Hoppel et al., 2005) is expected to enhance UV radiation and atmospheric oxidation potential in the troposphere (Jones et al., 2003). Nevertheless, the effects on

90   aerosols in the Antarctic troposphere have not been elucidated sufficiently. Because of the low aerosol number concentrations, direct effects of aerosol radiative forcing are negligible in the Antarctic (Bodhaine, 1995). After aerosol activation to cloud condensation nuclei (CCN), indirect effects might affect the atmospheric radiation budget and climate (Bromwich et al., 2012). With the present study, we are striving to understand the occurrence of NPF in the Antarctic, linkage among NPF, the ozone hole, and cloud properties in the Antarctic coast (around Syowa Station).

95   **2 Experiments and analysis**

2.1 Aerosol measurements at Syowa station, Antarctica

Aerosol measurements were taken during the 45th–47th Japanese Antarctic Research Expedition (2004–2006) at Syowa Station, Antarctica (69.0 °S, 39.0 °E), located on East Ongul Island in Lützow Holm Bay. Size distributions of ultrafine particles (diameter (D_p): 5 – 168 nm) were measured using SMPS (3936-N-25; TSI Inc.) during February 2004 – December

100   2006. A condensation particle counter (CPC) was used (3025A; TSI Inc.) to take SMPS measurements. Each scan for SMPS measurements took 5 min. CN concentrations (D_p >10 nm) was monitored using CPC 3010 (TSI Inc.) and was recorded every minute. In addition, an optical particle counter (OPC: KC22B; Rion Co. Ltd.) was used for measurements of size distributions of aerosols with size of D_p >0.08, >0.1, >0.2, 0.3, and >0.5 μm during January 2005 – December 2006. In OPC measurements, number concentrations were recorded every minute. SMPS, CPC, and OPC were operated at room temperature of ca. 20 °C in

105   the clean air observatory located at the windward side ca. 400 m distant from the main area of the station, where a diesel generator was operated. When winds came from the main area, local contamination might have occurred. Before analysis and discussion, locally contaminated data were screened using condensation nuclei concentrations (measured as aerosol monitoring at Syowa Station) and wind data (provided by the Japanese Meteorological Agency). Data screening procedures and criteria were identical to those described in earlier reports (Hara et al., 2011b, 2019). After screening of locally contaminated data,

110   daily mean aerosol number concentrations and size distributions were calculated for data analysis. Because of lower aerosol number concentrations during winter – early spring, hourly-mean aerosol size distributions through the year were obtained hardly to identify NPF and to analyze growth rate after NPF. Thus, daily mean aerosol size distribution was analyzed and discussed in the present study. Details of respective NPF events during the periods with higher aerosol concentrations will be discussed elsewhere. Aerosol sampling for chemical analysis was made using a two-stage mid-volume impactor and a back-

115   up filter. Water soluble aerosol constituents such as Na$^+$, SO$_4^{2-}$, and CH$_3$SO$_3^-$ were determined using ion chromatography. Details of aerosol sampling and chemical analysis were given in reports of our earlier work (Hara et al., 2004, 2018).

2.2 Data analysis

2.2.1 Estimation of coagulation sink and condensation sink

Nano-size aerosol particles are removed rapidly through coagulation. To elucidate the removal speed by coagulation,

120   coagulation sink (*Coag.S*) was calculated using the following equation (Kulmala et al., 2001).

$$\text{Coag.S} = \sum_j K_{ij} N_j \ (1)$$

Therein, K_{ij} and N_j respectively represent the coagulation coefficient in the transitional regime and the number concentrations of the size bin of j.

Condensation sink (*Cond.S*) was calculated to elucidate the removal speed of condensable vapours by condensation on aerosol particles using the following equation (Kulmala et al., 2001).

$$Cond.S = 4\pi D \int_0^\infty r\beta_M(r) \ n(r)dr = \sum_i \beta_M r_i \ N_i \ (2),$$

where r and β_M indicate particle radius and the transitional correction factor given by the following equation.

$$\beta_M = \frac{Kn+1}{0.377Kn+1+\frac{4}{3}\alpha^{-1}Kn^2+\frac{4}{3}\alpha^{-1}Kn} \ (3).$$

Here, *Kn* and α represent Knudsen number and the sticking coefficient. Value of α is assumed to be unity. *Kn* is expressed by

$$Kn = \frac{\lambda}{r} \ (4).$$

In equation (4), λ is mean free path. Details of calculation procedures were presented in an earlier report (Kulmala et al., 2001).

2.2.2 Estimation of the nucleation rate of aerosol particles

The nucleation rate of aerosol particles (D_p = 5 nm: J_5) was estimated as elucidating NPF and particle growth in the Antarctic troposphere. Number concentrations (*N*) of nano-size aerosol particles in each size bin depend on (1) growth from the smaller size by vapor condensation, (2) coagulation loss, and (3) growth to larger size by condensation. To calculate J_5, three size bins based on particles were used: D_p 1–5 nm, 5–10 nm, and 10–20 nm (Fig. 1). The change of the number concentrations in each size bin can be given by the following equation using *Coag.S* and the condensation growth rate (*Cond*) in accordance with Dal Maso et al. (2002).

$$\frac{dN_{1-5}}{dt} = J_1 - Coag.S_{1-5}N_{1-5} - Cond_{1-5}N_{1-5} \ (5)$$

$$\frac{dN_{5-10}}{dt} = J_5 - Coag.S_{5-10}N_{5-10} - Cond_{5-10}N_{5-10} \ (6)$$

$$\frac{dN_{10-20}}{dt} = J_{10} - Coag.S_{10-20}N_{10-20} - Cond_{10-20}N_{10-20} \ (7)$$

In this procedure, the flux of condensation growth to next size bin (*Cond$_i$N$_i$*) in *i* bin corresponds to J_{i+1}. From equations (5) – (7), J_5 give the following equations, assuming that $Cond_{10-20}N_{10-20}$ was negligible to estimate J_5.

$$J_5 = \frac{(Coag.S_{5-10}+Cond_{5-10})}{Cond_{5-10}}\left[\frac{\Delta N_{10-20}}{\Delta t} + Coag.S_{10-20}N_{10-20}\right] \ (8)$$

160   In this study, growth rate after NPF was not estimated in respective NPF events, as stated above. Here, growth rate ($0.01 - 1$ nm h^{-1}) and $\Delta N_{10-20} = 0$ was assumed to estimate J_5. Therefore, J_5 is obtainable from $Coag.S_{5-10}N_{5-10}$, $Cond_{5-10}$, and $Coag.S_{10-20}N_{10-20}$. Details of procedures for estimation of $Cond_{5-10}$ were described by Dal Maso et al. (2002). It is noteworthy that primary emissions of ultrafine aerosol particles can engender false estimation of J_5. Sea-salt particles were dominant even among ultrafine aerosol particles under storm conditions that prevailed during winter–spring at Syowa Station (Hara et al., 2011b).

165   Indeed, high J_5 was identified occasionally in the high contribution of sea-salt particles during winter.

2.2.3 Lognormal fitting of aerosol size distributions

Multi-modal fitting analysis of aerosol size distributions is used commonly to understand and discuss microphysical processes in the atmosphere. In this study, daily mean aerosol size distributions were approximated by a lognormal function, which is given by the following equation.

170

$$\frac{dN}{dlogD_p} = \sum_{i=1}^{n} \frac{N_i}{\sqrt{2\pi}log\sigma_i} exp\left[-\frac{(logD_p - logD_{p,i})}{2log^2\sigma_i}\right] \quad (9)$$

In equation (9), D_p, n, $D_{p,i}$, σ_i, and N_i respectively denote the particle diameter, mode number ($n = 1$–4), modal mean diameter in mode i, modal standard deviation in mode i, and the aerosol number concentrations in mode i. Lognormal fitting was

175 performed using the nls.lm function of minpack.lm library of R (R interface to the Levenberg–Marquardt nonlinear least-squares algorithm found in MINPACK). To avoid unrealistic lognormal fitting, we set the following restrictions: (1) $N_i > 1\%$ of total particle concentrations, (2) $1.2 \leq \sigma_i \leq 2.2$, and (3) $1.3 \, D_{p,i} < D_{p,i+1}$. The daily mean aerosol size distributions ($D_p = 5$–168 nm: SMPS only) were approximated by lognormal functions in 2004. The size distributions ($D_p = 5$–300 nm: SMPS + OPC) were analyzed by lognormal fitting in 2005–2006. For this study, we defined each mode based on the particle size range

180 as follows: fresh nucleation mode ($D_p < 10$ nm), aged nucleation mode ($D_p = 10$–25 nm), first Aitken mode ($D_p = 25$–50 nm), second Aitken mode ($D_p = 50$–100 nm), and accumulation mode ($D_p > 100$ nm).

2.3 Backward trajectory analysis

The 120-hr (5-day) backward trajectory was computed using the NOAA-HYSPLIT model

185 (https://ready.arl.noaa.gov/HYSPLIT.php) with the NCEP meteorological dataset (reanalysis) in model vertical velocity mode. The initial point was at 500 m above ground level over Syowa Station, Antarctica, because trajectory at lower altitudes has high uncertainty due to topographical affection and turbulence. According to tethered balloon measurements at Syowa (Hara et al., 2011a), top of boundary layer over Syowa was identified below 1400 m above ground level (annual mean, 840 m). For this study, we use the following criteria to divide each air mass origin: marine, <66 °S; coastal, 66–75°S; Antarctic-continental,

190 >75 °S; boundary layer (BL), <1500 m; and free troposphere (FT), >1500 m. Then, the time passing in each area such as marine BL (MBL), coastal BL, continental BL, continental FT, coastal FT, and marine FT (MFT) was counted for each backward trajectory. Areas with air masses staying for the longest times in the 5-day backward trajectory were classified into air mass origins.

3 Results and Discussion

195 **3.1 Aerosol size distributions**

Figure 2 presents examples of number size distributions of aerosol particles observed at Syowa Station. Our measurements show size distributions of ultrafine aerosol particles with mono-, bi-, tri-, and quad-modal structures. In earlier studies (Järvinen

et al., 2013; Weller et al., 2015), multi-modal aerosol size distributions with mono-, bi- and tri-modal structures were identified in the Antarctic. Although quad-modal structures were observed in this study, they were not reported in the earlier works. Quad-modal distributions were identified clearly in the present study, because the daily-mean aerosol size distributions were analyzed in this study in contrast to hourly-mean distributions in earlier works (Järvinen et al., 2013; Weller et al., 2015).

To characterize the aerosol size distributions, we compare the modal size in each mode (Fig. 3). In mono-modal distributions, the modal size ranged mostly in 40–105 nm. In bi-modal structures, the respective modal sizes in first and second modes were distributed in 20–40 nm and 60–135 nm. In tri-modal distributions, first–third modal sizes appeared in 8–20, 20–63, and 65–135 nm, respectively. Quad-modal structure had respective modal sizes of 7–13, 14–30, 30–65, and 70–140 nm. Mono-modal structure was observed often under storm and strong wind conditions with blowing snow during winter – early spring (Hara et al., 2011b, 2020). In these conditions, sea-salt particles in ultrafine – coarse modes were released from snow and sea-ice surface in polar regions (Hara et al., 2011b, 2014; 2017, 2020; Frey et al., 2020). In bi-modal distributions, modal sizes in the modes of the smallest modal size were greater than those in tri- and quad-modal distributions, so that bi-modal distributions were well-aged relative to tri- and quad-modal distributions. In the tri- and quad-modal structures, modal sizes in the smallest mode appeared mostly in diameter smaller than 20 nm. As shown by Asmi et al. (2010), Kyrö et al. (2013), Järvinen et al. (2013), Weller et al. (2015), Jokinen et al. (2018), and Kim et al. (2019), aerosol particles were grown to a few ten nm immediately after NPF even in the Antarctic troposphere during summer. Because the smallest mode appeared with diameter smaller than 20 nm, occasionally smaller than 10 nm, in tri-modal and quad-modal structures, aerosol size distributions with tri-modal and quad-modal structures might be associated with NPF and growth by vapor condensation. In bi-, tri-, and quad-modal structures, the modal sizes with the modes with the largest modal sizes had similar diameter larger than 50 nm, which corresponded to critical diameter for CCN activation in the Antarctic (Asmi et al., 2010).

Figure 4 shows the seasonal variation of abundance of modal structures at Syowa Station during our measurements. Mono-modal structure was identified mostly in May – August. Abundance of mono-modal structure was 16 – 60 % of days (mean, 37 %) during winter. As stated above, mono-modal structure during winter – early spring were associated with emission of sea-salt aerosols. Indeed, sea-salt aerosols released from sea-ice area were dominant during winter – early spring at the Antarctic coasts (e.g., Hara et al., 2012, 2013, 2020; Frey et al., 2020). Although bi-modal structure was observed through the year, abundance of bi-modal structure was 23 – 76 % (mean, 56 %) in April - September and 9 – 52 % (mean, 26 %) in December – March. Particularly, abundance of mono-modal and bi-modal structures were dominant (more than 90 %) in May–August. High abundance of tri-modal structure (14 – 75 %, mean 45 %) was observed in September–April. Particularly, abundance of tri-modal structures exceeded 50% in January–March. Surprisingly, tri-modal structures were identified even in winter (May–August) in spite of lower solar radiation (i.e., polar night). Modal sizes in the smallest mode of tri-modal structure were larger in winter than those in spring–summer (details will be presented in a later section). It is noteworthy that the quad-modal structure was found not only in December–February, but also in August–November and March–April. Considering the modal size in the smallest mode of quad-modal distributions, NPF might proceed in August–April in the Antarctic. Indeed, CN concentrations started to increase in August, with high concentrations in October–February at the coastal stations (e.g., Hara et al., 2011a, Weller et al., 2011; Asmi et al., 2013).

3.2 Relation between modal structures and air mass history

Annual cycles of air mass origins in each modal structure using 120-hr backward trajectory analysis are shown in Figure 5 for comparison between the modal structure and air mass history. Regarding general features of air mass origins in February 2004 – December 2006, coastal BL was dominant in summer (Fig. 5a), whereas abundance of continental FT increased during winter.

The seasonal cycles of air mass origins in 2004 – 2006 showed good agreement with long-term analysis of air mass origins at Syowa during 2005–2016 (Hara et al., 2019).

Seasonal features of air mass origins in mono-modal distributions (Fig. 5b) were similar to the general features (Fig. 5a), although the abundance of coastal FT was slightly higher in August and October. Considering that mono-modal structures corresponded mostly to storm conditions and strong winds during winter–spring (Hara et al., 2010, 2011b, 2020), the appearance of mono-modal structure were associated with primary emissions of sea-salt aerosols from the snow surface on sea-ice by strong winds rather than air mass history (i.e., transport pathway), as presented by Hara et al. (2012, 2013, 2020).

Similarly, seasonal features of air mass origins in bi-modal structure (Fig. 5c) resembled the general features. In general, bi-modal structures were recognized as well-aged distributions by condensation growth, coagulation, and cloud processes. Therefore, the appearance of bi-modal structures might be compared only slightly to air mass origins classified by 120-hr backward trajectory analysis.

In the tri-modal structure (Fig. 5d), the abundance of continental FT and coastal FT increased in spring, compared to the general features (Fig. 5a). Similarly to bi-modal structures, the appearance of some tri-modal structures, particularly with larger modal size (e.g., D_p>20 nm) in the smallest mode needed aging processes for a longer time. Consequently, seasonal variations of air mass origins in tri-modal structures were similar to general features, although sum of abundance of continental FT and coastal FT exceeded 50–60 % in August – October. This abundance was slightly higher than that of the general features.

Unlike the features in mono-modal, bi-modal, and tri-modal structures, continental FT and coastal FT were the most abundant air mass origins in quad-modal structures during spring and autumn (Fig. 5e). In general, features of air mass origins (Fig. 5a), MBL and coastal BL showed an important contribution during spring and autumn. Nevertheless, quad-modal structures in spring and autumn were identified only in the air mass from continental FT and coastal FT. This feature implies strongly that NPF proceeded in FT during spring and autumn in the Antarctic. In contrast to the high contributions of continental FT and coastal FT during spring and autumn, quad-modal structures were observed also in MBL and coastal BL during summer. Therefore, NPF might occur also in MBL and coastal BL during summer, as reported from results of earlier works (Weller et al., 2011; Asmi et al., 2013; Lachlan-Cope et al., 2020).

From aspects of location where NPF occur in the Antarctic troposphere, seasonal features of abundance of tri- and quad-modal distributions and their air mass origins were compared in Figure 6. Abundance of tri- and quad-modal distributions reflects on frequency of NPF in the Antarctic troposphere, although appearance of tri- and quad-modal distributions does not necessarily mean fresh or local NPF events near Syowa in this study. The abundance of tri- and quad-modal distributions was less than 10 % of days during May – August. In September – January, the abundance of tri- and quad-modal distributions was 40 – 48 % (mean, 44 %). By contrast, the abundance reached to 60 and 84 % in February and March. Seasonal features of NPF occurrence with high in spring – summer and minimum in winter were observed at Concordia (Järvinen et al., 2013) and King Sejong (Kim et al., 2019). The abundance (frequency) of the NPF, however, was largely varied at Syowa, Concordia and King Sejong. Difference of the abundance of NPF occurrence among Syowa, Concordia, and King Sejong might result from different atmospheric conditions such as the concentrations of aerosols and precursors, and different criteria for identification of NPF-growth events.

Abundance of tri- and quad-distributions with air mass origins of coastal FT and continental FT (Figure 6) ranged in 14 – 27 % of days (mean, 22 %) during September – November, in 8 – 16 % (mean, 11 %) during December – February, and in 11 –

32 % (mean, 22 %) during March – April. Particularly, fresh NPF (quad-modal size distributions) was identified in FT (12 % of days) during September – October and March, in contrast to 1 % in BL. Abundance of quad-modal distribution decreased to 3 % in FT during December – February. Considering high abundance of the quad-modal distributions in the air masses from

285   free troposphere in September – October (Figure 5e), spring NPF might occur dominantly in FT. On the other hand, abundance of tri- and quad-distributions with air mass of MBL and coastal BL increased (27 – 52%, mean 41 %) in BL during December – March. Abundance of quad-modal distributions in BL increased to 7 % in BL (3 % in FT) during December – February. In addition to NPF in FT, the high abundance in BL during December – March implies that more NPF proceeded in the BL during summer as pointed out by earlier works (Koponen et al., 2003; Virkkula et al., 2007; Asmi et al., 2010; Kyrö et al., 2013;

290   Weller et al., 2015; Jokinen et al., 2018; Kim et al., 2019; Jang et al., 2019; Lachlan-Cope et al., 2020). It is noteworthy that the abundance of continental FT and coastal FT during summer decreased remarkably, even in general features (Fig. 5a). Furthermore, the quad-modal structure was observed in continental FT and coastal FT in December (summer). CN enhancement by NPF and growth was observed in the lower free troposphere over Syowa Station during summer (Hara et al., 2011a). Therefore, the difference of contributable air mass origins in quad-modal structures between spring–autumn and

295   summer might reflect not only the locations of NPF occurrence but also seasonal features of general air mass origins (Fig. 5a). Consequently, NPF might occur in dominantly FT and partly BL during spring and autumn, and in BL and FT during summer.

3.3 Seasonal variations of aerosol physicochemical properties

Figure 7 depicts seasonal variations of all of the following: (a) concentrations of major aerosol constituents in D_p <200 nm; (b) CN concentrations; (c) modal sizes and number concentrations of each mode; (d) aerosol number concentrations of fresh

300   nucleation mode (D_p = 5–10 nm); (e) coagulation sinks and condensation sinks; (f) nucleation rates of aerosol particles with D_p = 5 nm (J_5); (g) extent of the Antarctic ozone hole; and (h) UV radiation near the surface at Syowa Station. Major water-soluble aerosol constituents of less than D_p = 200 nm are $CH_3SO_3^-$ and non-sea-salt (nss) SO_4^{2-} in summer and sea-salt (e.g., Na^+) in winter (Fig. 7a). The $CH_3SO_3^-$ concentrations, which start increasing at the end of August–September, show maximum concentrations in February–March at Syowa Station. Seasonal variation of $CH_3SO_3^-$ concentrations implies that oceanic

305   bioactivity and atmospheric photochemistry contribute to the maintenance of aerosol systems in September – early April because precursors of $CH_3SO_3^-$ (e.g., dimethylsulfide, DMS) derive from oceanic bioactivity (e.g., Minikin et al., 1998; Enami et al., 2016).

Variations of CN concentrations (Fig. 7b) showed clear seasonal features with minimum in winter and maximum in summer.

310   During winter, CN concentrations increased occasionally under storm and strong wind conditions. Increase of CN concentration from winter minimum started in end-August – early September at Syowa. CN concentrations and the seasonal features were similar to those measured at other coastal stations (e.g., Weller et al., 2011; Fiebig et al., 2014).

Our measurements show size distributions of ultrafine aerosol particles with mono-, bi-, tri-, and quad-modal structures (Fig.

315   2). The presence of tri-modal and quad-modal structures during spring–autumn suggests the frequent occurrence of NPF and growth in the atmosphere. Indeed, fresh-nucleation and aged-nucleation modes (D_p: <10 nm and 10–25 nm) appeared often in spring–summer (Fig. 7c). Particularly, most of fresh nucleation mode appeared in end-August – early October and February–March. Furthermore, the modal sizes increased gradually from fresh nucleation mode to first Aitken mode (D_p = 25–50 nm) in September–December. Such a gradual size shift implies that aerosol particles derived from NPF grew by the condensation

320   of condensable vapors such as H_2SO_4.

Aerosol number concentrations of D_p = 5–10 nm ($N_{5–10}$) show three maxima in September–October, December, and February–March (Fig. 7d) when tri-modal and quad-modal structures appeared frequently. These periods respectively correspond to the

appearance of the ozone hole (September–October marked by grey-shaded bands), the maximum of solar radiation (summer solstice marked by blue-shaded bands), and the minimum of the sea ice extent (February–March marked by green-shaded bands). In general, N_{5-10} was controlled by (1) NPF and growth from smaller size (ca. 1 nm), (2) coagulation loss, and (3) particle growth to larger sizes by vapor condensation. Additionally, J_5 showed three maxima similar to N_{5-10} variation (Fig. 7f). The estimated J_5 values in this study were comparable to the formation rate measured/estimated at Aboa (Kyrö et al., 2013), Neumayer (Weller et al., 2015), and Concordia (Järvinen et al., 2013), although high formation rate was obtained in the Antarctic Peninsula (Kim et al., 2019). In this study, high J_5 was observed often during May – August. However, this phenomenon might derive from dispersion of sea-salt aerosols from sea-ice areas by strong winds (Hara et al., 2011b). Therefore, high J_5 in the spring and summer are expected to be related to NPF.

The high J_5 and N_{5-10} in December and February–March are explainable by photochemical reactions, which form condensable vapors, and by the source strength of aerosol precursors released from oceanic bioactivity near the sea–ice margin. Indeed, high concentrations of DMS released from oceanic bioactivity were observed near sea-ice margins (Koga et al., 2014). By contrast, the sea–ice extent showed a maximum in spring (September – November, Fig. 7g). Consequently, other factors affecting the likelihood of high J_5 and N_{5-10} in spring should be considered. To elucidate the presence of fresh nucleation mode in spring, the location at which NPF occurred in the Antarctic region must be discussed. Air masses having quad-modal structures with fresh nucleation mode originated mostly from the upper FT over the Antarctic continent (Supplementary, Fig. S1). *Coag.S* of $D_p = 5$ nm aerosol particles increased gradually from 2×10^{-6} s^{-1} to 10^{-5} s^{-1} during September–December (Fig. 7e). From *Coag.S*, we estimated the e-folding time of the particles ($D_p = 5$ nm) by coagulation loss to 3.9–5.8 days in early September and 1.2–1.4 days in December (Supplementary, Fig. S2). This finding implies that the particles in the fresh nucleation mode observed at Syowa had too short a lifetime to be supplied by long-range transport from the mid-latitudes via the FT. Therefore, NPF should start in the Antarctic FT already by end-August.

Generally speaking, NPF is more likely to occur under conditions with (1) lower number concentrations of preexisting particles, (2) higher concentrations of condensable vapors, and (3) presence of sufficient photochemical oxidants such as OH. Because of low aerosol number concentrations in the Antarctic FT (Hara et al., 2011a), NPF can proceed preferentially in the FT if condensable vapor is present. Previous studies presented that the following condensable vapors participate in tropospheric NPF: H_2SO_4, CH_3SO_3H, NH_3, iodine species such as HIO_3, and amines (Yu et al., 2012; Kulmala et al., 2013; Kyrö et al., 2013; Weller et al., 2015; Simplä et al., 2016; Jen et al., 2016; Jokinen et al., 2018; Shen et al., 2019; Burrell et al., 2019). Actually, these vapors were identified in the Antarctic coasts and Southern Ocean (Jefferson et al., 1998a, 1998b; Simplä et al., 2016; Jokinen et al., 2018; Dall'Osto et al., 2019). High contribution of photochemical processes in the atmosphere was required to an important relation among J_5, aerosol size distributions, and CN concentrations. In addition, condensable vapors can be removed by condensation onto pre-existing particles. Therefore, the condensable vapors must be formed in FT, if NPF occurs in FT. Particularly, H_2SO_4, CH_3SO_3H, and iodine species such as HIO_3 were converted from precursors via photochemical reactions (e.g., Enami et al., 2016; Saiz-Lopez et al., 2008, 2011, 2014, 2016). To our knowledge, direct measurements of these vapors and their precursors have never been made in the Antarctic FT.

Atmospheric iodine cycles relate closely to snowpack chemistry in the Antarctic (e.g., Atkinson et al., 2012; Roscoe et al., 2015; Saiz-Lopez et al., 2015; Hara et al., 2020). Because of fast reactions of reactive iodine species (I_xO_y; e.g., Saiz-Lopez et al., 2008; Atkinson et al., 2012; Roscoe et al., 2015), atmospheric chemical processes of I_xO_y proceeds dominantly near surface (below 100 m). Hara et al. (2014) showed that significant injection of sea-salt aerosols originated from sea-ice area into free troposphere. Considering that sea-salts in snow and frost flowers on seasonal sea-ice had iodine enrichment by sea-salt fractionation (Hara et al., 2017), the rapidly vertical mixing of sea-salt particles as shown by Hara et al. (2014) play an

important role to supply iodine (mostly iodide) in aerosols into the free troposphere. Although heterogeneous reactions on sea-salt particles containing iodine during transport can engender I_xO_y release and formation of the iodine condensable vapors such as HIO_3. High concentrations of sea-salt particles, however, may prevent NPF by the iodine condensable vapors in free troposphere, because of efficient condensation loss of the vapors onto sea-salt aerosols.

DMS measurements at Concordia suggested that DMS was transported from coastal area (or ocean) to the inland station via FT (Preunkert et al., 2008). Therefore, photochemical reactions with DMS, H_2SO_4, and CH_3SO_3H might occur in the FT over the Antarctic continent. Sufficient photochemical oxidants such as OH and UV radiation are necessary for the conversion of condensable vapors such as DMS and SO_2. Appearance of O_3 hole in the Antarctic stratosphere can lead to UV enhancement with wavelength shorter than 310 nm even in the Antarctic troposphere during September – November. Therefore, atmospheric OH in the Antarctic troposphere is producible by UV radiation ($\lambda \leq 310$ nm) (Matusmi et al., 2002; Matsumi and Kawasaki, 2003).

Polar sunrise in the upper free troposphere occurs earlier than near the surface. Additionally, the appearance of the ozone hole enhances UV radiation, even in the troposphere during September–November (Figs. 7g-h). More noteworthy is the higher UV with wavelength shorter than 305 nm in October–November than in December near the surface at Syowa. For example, monthly-mean UV radiation in 300 – 305 nm at Syowa were 0.080, 0.098, and 0.068 kJ m^{-2} in October, November, and December, respectively. In general, light intensity including UV radiation is greater at higher altitudes because of atmospheric scattering and absorption. Considering the greater amount of UV radiation in the upper troposphere during September – November, the appearance of the ozone hole might enhance the formation of photochemical oxidants (e.g., OH) and condensable vapors, which then engender NPF in the upper troposphere (Figs. 7c-d).

3.4 Vertical variations of aerosol e-folding time by coagulation loss

After NPF, aerosol particles in fresh nucleation mode are grown mainly by condensation of condensable vapors and are coagulated efficiently onto pre-existing particles. For the better understanding on aerosol life cycle including microphysical processes in the Antarctic troposphere, aerosol lifetime must be discussed before discussion about relation between NPF and CCN ability. Williams et al. (2002) presented that aerosol particles with size of D_p <60 nm were removed dominantly by coagulation in FT. Therefore, vertical variations of e-folding time were estimated as aerosol lifetime in the Antarctic FT from *Coag.S* in each size (Fig. 7 e and Fig. S2). To our knowledge, aerosol size distributions in D_p <100 nm are still unknown in the Antarctic free troposphere through the year. Here, the e-folding time in FT was estimated, assuming that aerosol mixing ratio of aerosol number in respective size bins in FT was as same as that measured at surface. Aerosol size distributions in the air masses from coastal FT and continental FT and monthly-mean vertical profiles of air temperature measured Japan Meteorological Agency (URL: https://www.data.jma.go.jp/antarctic/datareport/index-e.html) were used in this estimation.

Figure 8 depicts vertical variations of the e-folding time of aerosol particles with sizes of $D_p = 1 - 50$ nm in September – December. In general, smaller aerosol particles has greater diffusion coefficient, so that the e-folding time was shorter particularly in D_p <10 nm. In other words, aerosol particles larger than $D_p = 20$ nm had longer e-folding time. Because of lower air temperature at higher altitudes, the estimated e-folding time tended to increase at the higher altitudes in all sizes and months. The e-folding time at upper troposphere (ca. 8.3 km, 300 hPa) was 3 – 4 times longer than that at surface. When aerosol particles were grown to the size larger than $D_p = 20 - 30$ nm, the e-folding time reached to >30 days in the middle – upper FT. In estimation of aerosol lifetime by Williams et al. (2002), aerosol lifetime was approximately 35 days in the upper FT and approximately 15 days in middle FT in the INDONEX campaign. It must be noticed that these lifetime by Williams et al.

(2002) was calculated from aerosol concentrations higher than those at surface of Syowa, and that the e-folding time in Fig. 8 was estimated based on aerosol size distributions measured at surface and constant mixing ratio. Tethered balloon measurements at Syowa (Hara et al., 2011) presented vertical gradient of CN concentrations with lower in FT (up to ca. 2500 m) except aerosol enhanced layer in lower FT. Additionally, aerosol number concentrations of particles with $D_p > 300$ nm in upper FT over Syowa were $1 - 2$ orders lower than those at surface (Kizu et al., 2010). With vertical gradient of the number concentrations of pre-existing particles, the e-folding time of $1 - 2$ months might be available and realistic for aerosol particles with size of $D_p > 20 - 30$ nm in the Antarctic free troposphere.

In contrast to longer e-folding time in the FT, the e-folding time was shorter in the BL (below 850 hPa) due to efficient coagulation loss. Particularly, the e-folding time at surface was shorter in the air masses originated from MBL and coastal BL than that in FT (not shown), because of high concentrations by primary emission of sea-salt aerosols in strong winds and NPF in MBL and coastal BL. In other words, high growth rate (i.e., high concentrations of condensable vapors) was required to particle growth for shorter periods (within the e-folding time) in BL. For example, under the conditions with growth rate of 0.05, 0.1, 0.2, 0.5 nm h^{-1}, it takes approximately 3.3 days, 1.7 days, 0.8 days, and 0.33 days for initial growth from $D_p = 1$ nm to 5 nm, respectively. Under the slow growth conditions, the time for initial growth exceeded the e-folding time of $D_p = 1$ and 5 nm in BL. In FT, however, aerosol particles can be survived for longer time under the conditions with slower particle growth (lower concentrations of condensable vapors) relative to those in BL. Consequently, aerosol particles can be grown gradually through condensation of condensable vapors in the Antarctic troposphere once new particles grow to the aged-nucleated particles ($D_p > 10$ nm). Finally, UV enhancement in the upper troposphere by the ozone hole in end-August – November might modify the aerosol population and size distributions in the Antarctic troposphere during spring–summer. Therefore, aerosol properties in the Antarctic troposphere during spring – summer are not "pristine" but under the Anthropocene conditions, although the Antarctic troposphere remains the cleanest on the earth.

3.5 CCN potential and cloud amount during summer

Gradual change of modal sizes in fresh nucleation mode and first Aitken mode were observed during spring–summer (Fig. 7c). When aerosol particles derived from NPF during the periods with appearance of O$_3$ hole grow to critical diameter, the aerosol particles can act as CCN. Here, aerosol particles grown after NPF during the periods with O$_3$ hole were focused to elucidate relation to CCN ability and CCN properties during summer. As shown in Figure 7c, modal sizes increased gradually in aged-nucleation mode and first Aitken mode from end-August till December. This gradual feature of the modal sizes was associated likely with particle growth after NPF. Measurements of aerosol hygroscopicity at Aboa showed that the critical diameter was approximately ca. 50 nm during summer (Asmi et al., 2010). Considering that gradual particle growth in the aged-nucleation and first Aitken modes (Fig. 7c), NPF during the periods with O$_3$ hole and growth are expected to link to cloud properties during summer. Therefore, we attempt to estimate the contribution of aerosols derived from NPF during the periods with O$_3$ hole to act as CCN in November–January based on the following assumptions: aerosol particles supplied from spring NPF were grown to aged-nucleation and first Aitken modes. For this estimation, the contribution to CCN (R_{CCN}) was defined as the ratio of the aerosol number concentrations of $D_p > 50$ nm in aged-nucleation and first Aitken modes ($N_{D>50}$) to the total aerosol number concentrations in $D_p > 50$ nm (total-$N_{D>50}$, Fig. 7). The value of R_{CCN} was estimated using the following equation.

$$R_{CCN}(\%) = \frac{N_{D>50}}{total-N_{D>50}} \times 100 \ (7)$$

Figure 9 depicts R$_{CCN}$ in the continental FT and coastal BL in November – January. ANOVA variance test indicated significant difference ($p = 0.0125$) between R$_{CCN}$ in the continental FT and coastal BL. Difference of aerosol size distributions are taken into account to ascertain R$_{CCN}$ in the continental FT and coastal BL. As shown in Figure S3, the modal size in the smallest

mode was smaller in BL than those in FT in December – January, although the modal size was insignificantly different in November. Aerosol particles with size of D_p <30 nm were supplied by NPF and growth, as mentioned above. Therefore, NPF in the BL in December – January might lead to the difference of the modal sizes in the smallest mode. The modal size in the smallest mode in the BL was smaller than the critical diameter. Therefore, aerosol particles supplied from summer NPF in the

455   BL were not grown sufficiently to the critical diameter by condensation. We infer that aerosol enhancement by NPF during the periods with appearance of O_3 hole might modify not only aerosol size distributions but also CCN ability and cloud properties in summer.

Trends of cloud amounts at Syowa Station were examined to assess impact of spring NPF enhanced by appearance of O_3 hole

460   on CCN ability and cloud properties during summer. Figure 10 depicts variations of cloud amounts in December and January since 1969. Although no increasing trend was identified for air temperature or water vapor concentrations related to the cloud amount, a marked increasing trend with p values lower than 0.01 was found only for December and January during 1969–2012. Particularly, the cloud amount at Syowa Station was significantly higher after the appearance of the O_3 hole (Fig. 10b, and Fig. S4). Consequently, the cloud amount trend during summer might result from spring NPF enhanced by O_3 hole

465   appearance. Because of the conformable relation between the cloud amount and radiative fluxes (Yamanouchi et al., 2007), UV enhancement by the O_3 hole can affect atmospheric radiation budgets by aerosol/cloud properties in the Antarctic during summer.

Our hypothesis is summarized as shown in the schematic figure (Fig. 11). In polar sunrise, solar radiation recovers earlier in

470   the stratosphere and the upper troposphere. Then, ozone depletion by catalytic reactions of chlorine cycle starts in the Antarctic stratosphere. Ozone hole appears in the Antarctic stratosphere from the end-August till end-November. Appearance of the ozone hole engenders UV enhancement and then production of atmospheric oxidants such as OH in the troposphere. Atmospheric oxidants such as OH prefer to be formed in the upper troposphere by UV enhancement. Condensable vapors (i.e., aerosol precursors with lower vapor pressure) are producible by photochemical oxidation. H_2SO_4 and CH_3SO_3H are one of the

475   most important condensable vapors for NPF and growth in the Antarctic FT. Also, NPF occurs already by end-August in the upper troposphere. As a consequence, NPF is enhanced in FT under UV enhancement by O_3 hole during spring (end-August–November). Aerosol particles in fresh nucleation mode grow gradually by the condensation of condensable vapors in the FT. Some aerosol particles in fresh and aged nucleation modes are transported to the lower troposphere in the Antarctic coasts. With condensation growth, some aerosol particles originated from spring NPF in the free troposphere can be grown to size

480   greater than the critical diameter (ca. 50 nm) in the summer. NPF proceed even in coastal and MBL from end-spring – summer. In contrast to FT, H_2SO_4, CH_3SO_3H, and other condensable vapors (e.g., HIO_3, NH_3, and amines) can lead to NPF and growth in BL. Aerosol particles originated from NPF in BL are efficiently removed by coagulation under the conditions with higher aerosol concentrations of pre-existing particles than those of FT except high growth rate. Consequently, lesser aerosol particles derived from summer NPF in the boundary layer grow up to the critical diameter than from spring NPF in the FT. Our results

485   demonstrate that spring NPF plays an important role in aerosol population and cloud properties in the summer under conditions with appearance of the Antarctic ozone hole. Knowledge on the following issues is required essentially in the future to ascertain our hypothesis; (1) aerosol size distributions of particles smaller than 100 nm in the FT, (2) chemical forms of the condensable vapors and their concentrations in the FT and BL, and (3) their vertical and seasonal variations in the Antarctic.

4. Conclusion

490   Aerosol measurements were made using SMPS and OPC at Syowa Station, Antarctica in 2004–2006. Aerosol size distributions had mono-, bi-, tri- and quad-modal distributions during our measurements. The mono-modal distribution was dominant under strong wind conditions during May–August. The bi-modal distribution was identified through the year. Tri- and quad-modal

distributions were observed mostly in September–April. Seasonal features of N_{5-10} and J_5 imply that NPF identified at Syowa Station was associated with UV enhancement by ozone hole appearance in spring, maximum of solar radiation in summer, and

495   minimum of sea-ice extent in February–March. Also, NPF occurs in FT during spring and autumn and in the free troposphere and boundary layer during summer. Additionally, spring NPF and particle growth are linked to cloud properties during summer.

We obtained direct evidence indicating that spring UV enhancement by the ozone hole engendered spring NPF and growth in the Antarctic FT. With recovery of the ozone hole (Solomon et al., 2016; Kuttippurath et al., 2017), aerosol properties and

500   populations might be modified for the next several decades. As a result, indirect effects on atmospheric radiation budgets and climate change in the Antarctic regions during the summer can revert to their levels which prevailed before the ozone hole appearance. More aerosol measurements in Antarctic regions must be taken to monitor these trends and future effects.

Data availability

Data are available by contacting the corresponding author (KH: harakei@fukuoka-u.ac.jp).

505   **Author contributions**

KH, KO, and TY designed aerosol measurements at Syowa Station. KH, KO, and MY conducted wintering aerosol measurements at Syowa Station in 2004–2006. KH and CNH contributed to data analysis including SMPS/OPC data and meteorological data. KH prepared the manuscript and led data interpretation. All co-authors contributed to discussions about data interpretation and the manuscript.

510   **Competing interests**

The authors declare that they have no conflict of interest.

520   **References**

Atkinson, H., Huang, -J R, Chance, R., Roscoe, H., Hughes, C., Davison, B., Schönhardt, A., Mahajan, A., Saiz-Lopez, A., Hoffmann, T., and Liss, P.: Iodine emissions from the sea ice of the Weddell Sea, *Atmospheric Chemistry and Physics*, 12, 11229-11244, https://doi.org/10.5194/acp-12-11229-2012, 2012.

Asmi, A., Coen, C. M., Ogren, J., Andrews, E., Sheridan, P., Jefferson, A., Weingartner, E., Baltensperger, U., Bukowiecki,

525   N., Lihavainen, H., Kivekäs, N., Asmi, E., Aalto, P., Kulmala, M., Wiedensohler, A., Birmili, W., Hamed, A., O'Dowd, C., Jennings, S., Weller, R., Flentje, H., Fjaeraa, A., Fiebig, M., Myhre, C., Hallar, A., Swietlicki, E., Kristensson, A. and Laj, P.: Aerosol decadal trends – Part 2: In-situ aerosol particle number concentrations at GAW and ACTRIS stations, *Atmospheric Chemistry and Physics*, 13, 895-916, doi:10.5194/acp-13-895-2013, 2013.

Bodhaine, B.A. Aerosol absorption measurements at Barrow, Mauna Loa and the South Pole. *Journal of Geophysical Research*: *Atmospheres,* **100**, 8967–8975 (1995).

Bromwich, D. H., Nicolas, J. P., Hines, K. M., Kay, J. E., Key, E. L., Lazzara, M. A., Lubin, D., McFarquhar, G. M., Gorodetskaya, I. V., Grosvenor, D. P., Lachlan-Cope, T., and van Lipzig, N. P.: Tropospheric clouds in Antarctica, *Reviews of Geophysics*, 50(1), doi:10.1029/2011RG000363, 2012.

Burrell, E., Kar, T. and Hansen, J. C.: Computational Study of the Thermodynamics of New Particle Formation Initiated by Complexes of H_2SO_4–H_2O–NH_x, CH_3SO_3H–H_2O–NH_x, and HO_2–H_2O–NH_x, *ACS Earth Space Chem.*, 3(8), 1415–1425, doi:10.1021/acsearthspacechem.9b00120, 2019.

Dall´Osto, M., Beddows, D. C. S., Tunved, P., Krejci, R., Ström, J., Hansson, H.-C., Yoon, Y. J., Park, K.-T., Becagli, S., Udisti, R., Onasch, T., O´Dowd, C. D., Simó, R., and Harrison, R. M.: Arctic sea ice melt leads to atmospheric new particle formation, *Scientific Reports*, 7(1), 3318, doi:10.1038/s41598-017-03328-1, 2017.

Dall'Osto, M., Airs, R. L., Beale, R., Cree, C., Fitzsimons, M. F., Beddows, D., Harrison, R. M., Ceburnis, D., O'Dowd, C., Rinaldi, M., Paglione, M., Nenes, A., Decesari, S., and Simó, R.: Simultaneous Detection of Alkylamines in the Surface Ocean and Atmosphere of the Antarctic Sympagic Environment, *Acs Earth Space Chem*, 3, 854–862, https://doi.org/10.1021/acsearthspacechem.9b00028, 2019.

Dal Maso, M., Kulmala, M., Lehtinen, K., Mäkelä, J., Aalto, P., and O'Dowd, C.: Condensation and coagulation sinks and formation of nucleation mode particles in coastal and boreal forest boundary layers, *Journal of Geophysical Research*, 107(D19), doi:10.1029/2001JD001053, 2002.

Fiebig, M., Hirdman, D., Lunder, C., Ogren, J., Solberg, S., Stohl, A., and Thompson, R.: Annual cycle of Antarctic baseline aerosol: controlled by photooxidation-limited aerosol formation, *Atmospheric Chemistry and Physics*, 14(6), 3083–3093, doi:10.5194/acp-14-3083-2014, 2014.

Frey, M. M., Norris, S. J., Brooks, I. M., Anderson, P. S., Nishimura, K., Yang, X., Jones, A. E., Mastromonaco, M. G., Jones, D. H., and Wolff, E. W.: First direct observation of sea salt aerosol production from blowing snow above sea ice, *Atmospheric Chemistry and Physics*, 20, 2549–2578, https://doi.org/10.5194/acp-20-2549-2020, 2020.

Gras, J. L. Condensation nucleus size distribution at Mawson, Antarctica: seasonal cycle. *Atmospheric Environment* **27**, 1417–1425 (1993).

Hara, K., Osada, K., Nishita-Hara, C., and Yamanouchi, T.: Seasonal variations and vertical features of aerosol particles in the Antarctic troposphere, *Atmospheric Chemistry and Physics*, 11, 5471-5484, doi:10.5194/acp-11-5471-2011, 2011a.

Hara, K., Osada, K., Nishita-Hara, C., Yabuki, M., Hayashi, M., Yamanouchi, T., Wada, M. and Shiobara, M.: Seasonal features of ultrafine particle volatility in the coastal Antarctic troposphere, *Atmospheric Chemistry and Physics*, 11, 9803-9812, doi:10.5194/acp-11-9803-2011, 2011b.

Hara, K., Osada, K., Yabuki, M., and Yamanouchi, T.: Seasonal variation of fractionated sea-salt particles on the Antarctic coast. *Geophys. Res. Lett*. **39**, L18801, doi:10.1029/2012GL052761, 2012.

Hara, K., Osada, K., and Yamanouchi, T.: Tethered balloon-borne aerosol measurements: seasonal and vertical variations of aerosol constituents over Syowa Station, Antarctica, *Atmospheric Chemistry and Physics*, 13, 91199139, https://doi.org/10.5194/acp-13-9119-2013, 2013.

Hara, K., Nakazawa, F., Fujita, S., Fukui, K., Enomoto, H., and Sugiyama, S.: Horizontal distributions of aerosol constituents and their mixing states in Antarctica during the JASE traverse, *Atmospheric Chemistry and Physics*, 14, 10211–10230, https://doi.org/10.5194/acp-14-10211-2014, 2014.

Hara, K., Matoba, S., Hirabayashi, M., and Yamasaki, T.: Frost flowers and sea-salt aerosols over seasonal sea-ice areas in northwestern Greenland during winter–spring, 17, *Atmospheric Chemistry and Physics*, 8577–8598, https://doi.org/10.5194/acp-17-8577-2017, 2017.

Hara, K., Osada, K., Yabuki, M., Takashima, H., Theys, N., and Yamanouchi, T.: Important contributions of sea-salt aerosols to atmospheric bromine cycle in the Antarctic coasts, *Scientific Reports*, 8(1), 13852, doi:10.1038/s41598-018-32287-4, 2018.

Hara, K., Sudo, K., Ohnishi, T., Osada, K., Yabuki, M., Shiobara, M., and Yamanouchi, T.: Seasonal features and origins of carbonaceous aerosols at Syowa Station, coastal Antarctica, *Atmospheric Chemistry and Physics*, 19(11), 7817–7837, doi:10.5194/acp-19-7817-2019, 2019.

Hoppel, K., Bevilacqua, R., Canty, T., Salawitch, R., and Santee, M.: A measurement/model comparison of ozone photochemical loss in the Antarctic ozone hole using Polar Ozone and Aerosol Measurement observations and the Match technique. *Journal of Geophysical Research*: *Atmospheres*, **110**, D19304, doi:10.1029/2004JD005651(2005).

Humphries, R., Klekociuk, A., Schofield, R., Keywood, M., Ward, J. and Wilson, S.: Unexpectedly high ultrafine aerosol concentrations above East Antarctic sea ice, *Atmospheric Chemistry and Physics*, 16(4), doi:10.5194/acp-16-2185-2016, 2016.

Järvinen, E., Virkkula, A., Nieminen, T., Aalto, P., Asmi, E., Lanconelli, C., Busetto, M., Lupi, A., Schioppo, R., Vitale, V., Mazzola, M., Petäjä, T., Kerminen, -M V and Kulmala, M.: Seasonal cycle and modal structure of particle number size distribution at Dome C, Antarctica, *Atmospheric Chemistry and Physics*, **13**(15), 7473-7487, doi:10.5194/acp-13-7473-2013, 2013.

Jefferson, A., Tanner, D., Eisele, F., and Berresheim, H.: Sources and sinks of H2SO4 in the remote Antarctic marine boundary layer, Sources and sinks of H_2SO_4 in the remote Antarctic marine boundary layer, *J. Geophys. Res.*, 103(D1), 1639– 1645, doi:10.1029/97JD01212, 1998a.

Jefferson, A., Tanner, D., Eisele, F., Davis, D., Chen, G., Crawford, J., Huey, J., Torres, A., and Berresheim, H.: OH photochemistry and methane sulfonic acid formation in the coastal Antarctic boundary layer, *J. Geophys. Res.*, 103(D1), 1647– 1656, doi:10.1029/97JD02376, 1998b.

Jen, C. N., Bachman, R., Zhao, J., McMurry, P. H. and Hanson, D. R.: Diamine-sulfuric acid reactions are a potent source of new particle formation, *Geophysical Research Letters*, 43(2), 867–873, doi:10.1002/2015gl066958, 2016.

Jokinen, T., Sipilä, M., Kontkanen, J., Vakkari, V., Tisler, P., Duplissy, E.-M., Junninen, H., Kangasluoma, J., Manninen, H. E., Petäjä, T., Kulmala, M., Worsnop, D. R., Kirkby, J., Virkkula, A., and Kerminen, V.-M.: Ion-induced sulfuric acid–ammonia nucleation drives particle formation in coastal Antarctica, *Science Advances*, 4, eaat9744, https://doi.org/10.1126/sciadv.aat9744, 2018.

Jones, A. and Wolff, E.: An analysis of the oxidation potential of the South Pole boundary layer and the influence of stratospheric ozone depletion. *Journal of Geophysical Research*, 108(D18), 4565, doi:10.1029/2003JD003379, 2003.

Kerminen, V.-M., Chen, X., Vakkari, V., Petäjä, T., Kulmala, M. and Bianchi, F.: Atmospheric new particle formation and growth: review of field observations, *Environmental Research Letters*, 13(10), 103003, doi:10.1088/1748-9326/aadf3c, 2018.

Kim, J., Yoon, Y. J., Gim, Y., Choi, J. H., Kang, H. J., Park, K.-T., Park, J., and Lee, B. Y.: New particle formation events observed at King Sejong Station, Antarctic Peninsula – Part 1: Physical characteristics and contribution to cloud condensation nuclei, *Atmospheric Chemistry and Physics,* 19, 7583–7594, https://doi.org/10.5194/acp-19-7583-2019, 2019.

Kizu, N., Hayashi, M., Yamanouchi, T., Iwasaka, Y., and Watanabe, M.: Seasonal and annual variations of aerosol concentrations in the troposphere and stratosphere over Syowa Station observed by a balloon-borne optical particle counter, *Antarctic Record*, 54, 760-778, doi/10.15094/00009583, 2010.

610 Koga, S., Nomura, D., and Wada, M.: Variation of dimethylsulfide mixing ratio over the Southern Ocean from 36°S to 70°S, *Polar Science*, 8, 306–313, https://doi.org/10.1016/j.polar.2014.04.002, 2014.

Kulmala, M., Kontkanen, J., Junninen, H., Lehtipalo, K., Manninen, H. E., Nieminen, T., Petäjä, T., Sipilä, M., Schobesberger, S., Rantala, P., Franchin, A., Jokinen, T., Järvinen, E., Äijälä, M., Kangasluoma, J., Hakala, J., Aalto, P. P., Paasonen, P., Mikkilä, J., Vanhanen, J., Aalto, J., Hakola, H., Makkonen, U., Ruuskanen, T., Mauldin, R. L., Duplissy, J., Vehkamäki,
615 H., Bäck, J., Kortelainen, A., Riipinen, I., Kurtén, T., Johnston, M. V., Smith, J. N., Ehn, M., Mentel, T. F., Lehtinen, K. E., Laaksonen, A., Kerminen, V.-M. and Worsnop, D. R.: Direct Observations of Atmospheric Aerosol Nucleation, *Science*, 339(6122), 943–946, doi:10.1126/science.1227385, 2013.

Kulmala, M., Maso, M., Mäkelä, J., Pirjola, L., Väkevä, M., Aalto, P., Miikkulainen, P., Hämeri, K. and O'Dowd, C.: On the formation, growth and composition of nucleation mode particles, *Tellus Series B-chemical and Physical Meteorology*,
620 doi:10.1034/j.1600-0889.2001.530411.x, 2001.

Kuttippurath, J. and Nair, P.: The signs of Antarctic ozone hole recovery, *Scientific Reports* **7**, 585, 2017.

Kyrö, M E, Kerminen, -M V, Virkkula, A., Maso, D. M., Parshintsev, J., Ruíz-Jimenez, J., Forsström, L., Manninen, H., Riekkola, -L M, Heinonen, P., and Kulmala, M.: Antarctic new particle formation from continental biogenic precursors, *Atmospheric Chemistry and Physics*, 13(7), 35273546, doi:10.5194/acp-13-3527-2013, 2013.

625 Jang, E., Park, K.-T., Yoon, Y. J., Kim, T.-W., Hong, S.-B., Becagli, S., Traversi, R., Kim, J., and Gim, Y.: New particle formation events observed at the King Sejong Station, Antarctic Peninsula – Part 2: Link with the oceanic biological activities, *Atmospheric Chemistry and Physics*. 19, 7595–7608, https://doi.org/10.5194/acp-19-7595-2019, 2019.

Matsumi, Y., Comes, F., Hancock, G., Hofzumahaus, A., Hynes, A., Kawasaki, M. and Ravishankara, A.: Quantum yields for production of O(^{1}D) in the ultraviolet photolysis of ozone: Recommendation based on evaluation of laboratory data, Journal
630 of Geophysical Research: Atmospheres (1984–2012), 107(D3), ACH 1-1-ACH 1-12, doi:10.1029/2001JD000510, 2002.

Matsumi, Y. and Kawasaki, M.: Photolysis of atmospheric ozone in the ultraviolet region, *Chem. Rev.* **103**, 4767–4782 (2003).

Millero, F., Feistel, R., Wright, D. and McDougall, T.: The composition of Standard Seawater and the definition of the Reference-Composition Salinity Scale. Deep Sea Research Part I: *Oceanographic Research Papers* **55**, 50–72 (2008).

Minikin, A., Legrand, M., Hall, J., Wagenbach, D., Kleefeld, C., Wolff, E., Pasteur, E., and Ducroz, F.: Sulfur-containing
635 species (sulfate and methanesulfonate) in coastal Antarctic aerosol and precipitation, *Journal of Geophysical Research*, doi:10.1029/98jd00249, 1998.

Preunkert, S., Jourdain, B., Legrand, M., Udisti, R., Becagli, S., and Cerri, O.: Seasonality of sulfur species (dimethyl sulfide, sulfate, and methanesulfonate) in Antarctica: Inland versus coastal regions, *Journal of Geophysical Research*, 113(D15), doi:10.1029/2008jd009937, 2008.

640 Read, K., Lewis, A., Bauguitte, S., Rankin, A., Salmon, R., Wolff, E., Saiz-Lopez, A., Bloss, W., Heard, D., Lee, J. and Plane, J.: DMS and MSA measurements in the Antarctic Boundary Layer: impact of BrO on MSA production, *Atmospheric Chemistry and Physics*, 8(11), 2985-2997, doi:10.5194/acp-8-2985-2008, 2008.

Roscoe, H. K., Jones, A. E., Brough, N., Weller, R., Saiz-Lopez, A., Mahajan, A. S., Schoenhardt, A., Burrows, J. P. and Fleming, Z. L.: Particles and iodine compounds in coastal Antarctica, Journal of Geophysical Research: Atmospheres,
645 120(14), 7144–7156, doi:10.1002/2015jd023301, 2015.

Saiz-Lopez, A., Plane, J., Mahajan, A., Anderson, P., Bauguitte, J.-B. S., Jones, A., Roscoe, H., Salmon, R., Bloss, W., Lee, J., and Heard, D.: On the vertical distribution of boundary layer halogens over coastal Antarctica: implications for O3, HOx, NOx and the Hg lifetime, *Atmospheric Chemistry and Physics*, 8, 887–900, https://doi.org/10.5194/acp-8-887-2008, 2008.

650   Saiz-Lopez, A., Plane, J. M., Baker, A. R., Carpenter, L. J., Glasow, R. von, Martín, J. C., McFiggans, G., and Saunders, R. W.: Atmospheric Chemistry of Iodine, *Chemical Reviews*, 112, 1773–1804, https://doi.org/10.1021/cr200029u, 2011.

Saiz-Lopez, A., Fernandez, R., Ordóñez, C., Kinnison, D., Martín, G. J., Lamarque, J.-F., and Tilmes, S.: Iodine chemistry in the troposphere and its effect on ozone, *Atmospheric Chemistry and Physics*, 14, 13119–13143, https://doi.org/10.5194/acp-14-13119-2014, 2014.

655   Saiz-Lopez, A., Blaszczak-Boxe, C., and Carpenter, L.: A mechanism for biologically induced iodine emissions from sea ice, *Atmospheric Chemistry and Physics*, 15, 9731–9746, https://doi.org/10.5194/acp-15-9731-2015, 2015.

Saiz-Lopez, A., Plane, J. M., Cuevas, C. A., Mahajan, A. S., Lamarque, J.-F., and Kinnison, D. E.: Nighttime atmospheric chemistry of iodine, *Atmospheric Chemistry and Physics*, 16, 15593–15604, https://doi.org/10.5194/acp-16-15593-2016, 2016.

660   Shen, J., Xie, H.-B., Elm, J., Ma, F., Chen, J., and Vehkamäki, H.: Methanesulfonic Acid-driven New Particle Formation Enhanced by Monoethanolamine: A Computational Study, Environ. Sci. Technol., 53(24), 14387–14397, doi:10.1021/acs.est.9b05306, 2019.

Sipilä, M., Sarnela, N., Jokinen, T., Henschel, H., Junninen, H., Kontkanen, J., Richters, S., Kangasluoma, J., Franchin, A., Peräkylä, O., Rissanen, M. P., Ehn, M., Vehkamäki, H., Kurten, T., Berndt, T., Petäjä, T., Worsnop, D., Ceburnis, D.,
665   Kerminen, V.-M., Kulmala, M. and O'Dowd, C.: Molecular-scale evidence of aerosol particle formation via sequential addition of HIO3, Nature, 537(7621), 532–534, doi:10.1038/nature19314, 2016.

Solomon, S., Ivy, D. J., Kinnison, D., Mills, M. J., Neely, R. R., and Schmidt, A.: Emergence of healing in the Antarctic ozone layer, Science, 353(6296), 269–274, doi:10.1126/science.aae0061, 2016.

Weller, R., Minikin, A., Wagenbach, D. and Dreiling, V.: Characterization of the inter-annual, seasonal, and diurnal variations
670   of condensation particle concentrations at Neumayer, Antarctica, Atmospheric Chemistry and Physics, 11(24), 13243-13257, doi:10.5194/acp-11-13243-2011, 2011.

Weller, R., Schmidt, K., Teinilä, K., and Hillamo, R. Natural new particle formation at the coastal Antarctic site Neumayer, *Atmospheric Chemistry and Physics*, 15, 11399–11410, 2015.

Williams, J., Reus, M. de, Krejci, R., Fischer, H., and Ström, J.: Application of the variability-size relationship to atmospheric
675   aerosol studies: estimating aerosol lifetimes and ages, *Atmospheric Chemistry and Physics*, 2, 133–145, https://doi.org/10.5194/acp-2-133-2002, 2002.

Yamanouchi, T. and Shudou, Y. Trends in cloud amount and radiative fluxes at Syowa Station, Antarctica. *Polar Science* **1**, 17–23 (2007).

Yu, H., McGraw, R. and Lee, S.-H.: Effects of amines on formation of sub-3 nm particles and their subsequent growth,
680   Geophysical Research Letters, 39, doi:10.1029/2011gl050099, 2012.
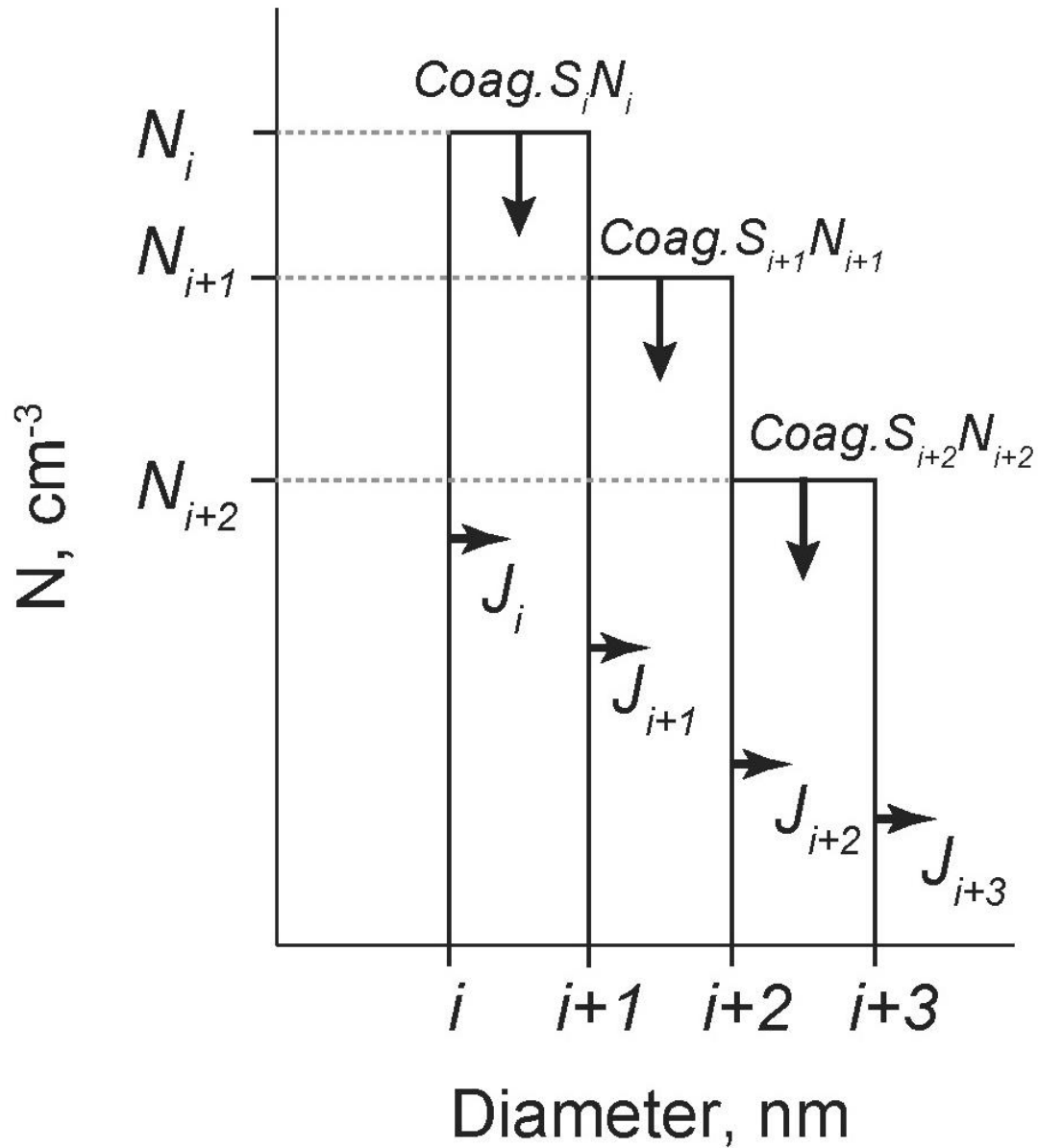
Figure 1: Schematic figure showing procedures used for the nucleation rate of aerosol particles with size of $D_p = 5$ nm (J_5). N_i,
$Coag.S_i$, and J_i indicate the number concentrations, coagulation sink and growth (or formation) rate in each size bin.
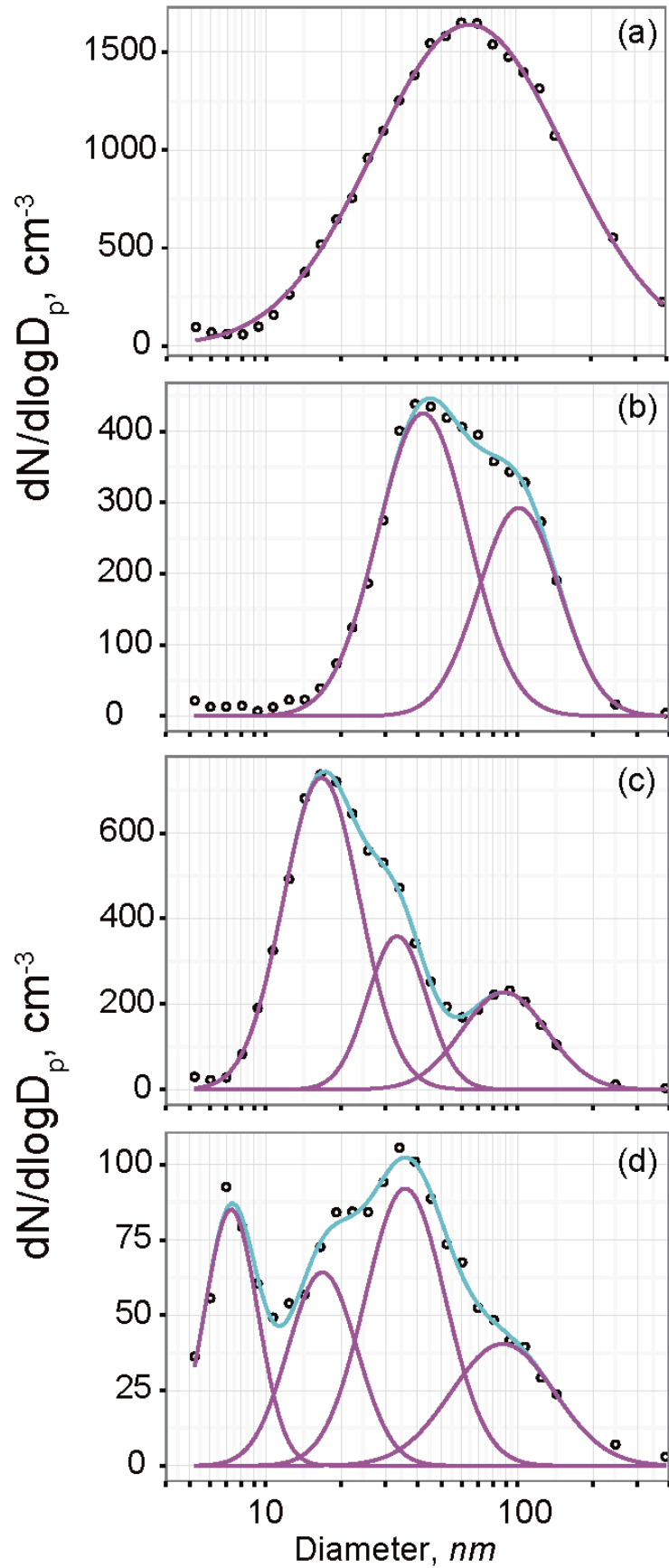
Figure 2: Examples of aerosol size distributions with (a) mono-modal (3 May 2005), (b) bi-modal (4 March 2005), (c) tri-modal (14 February 2005), and (d) quad-modal (8 September 2006) structures. Circles, pink lines, and cyan lines in (a–d), respectively show the number concentrations in each mode by approximated by lognormal fitting, and total concentrations of the respective modes.
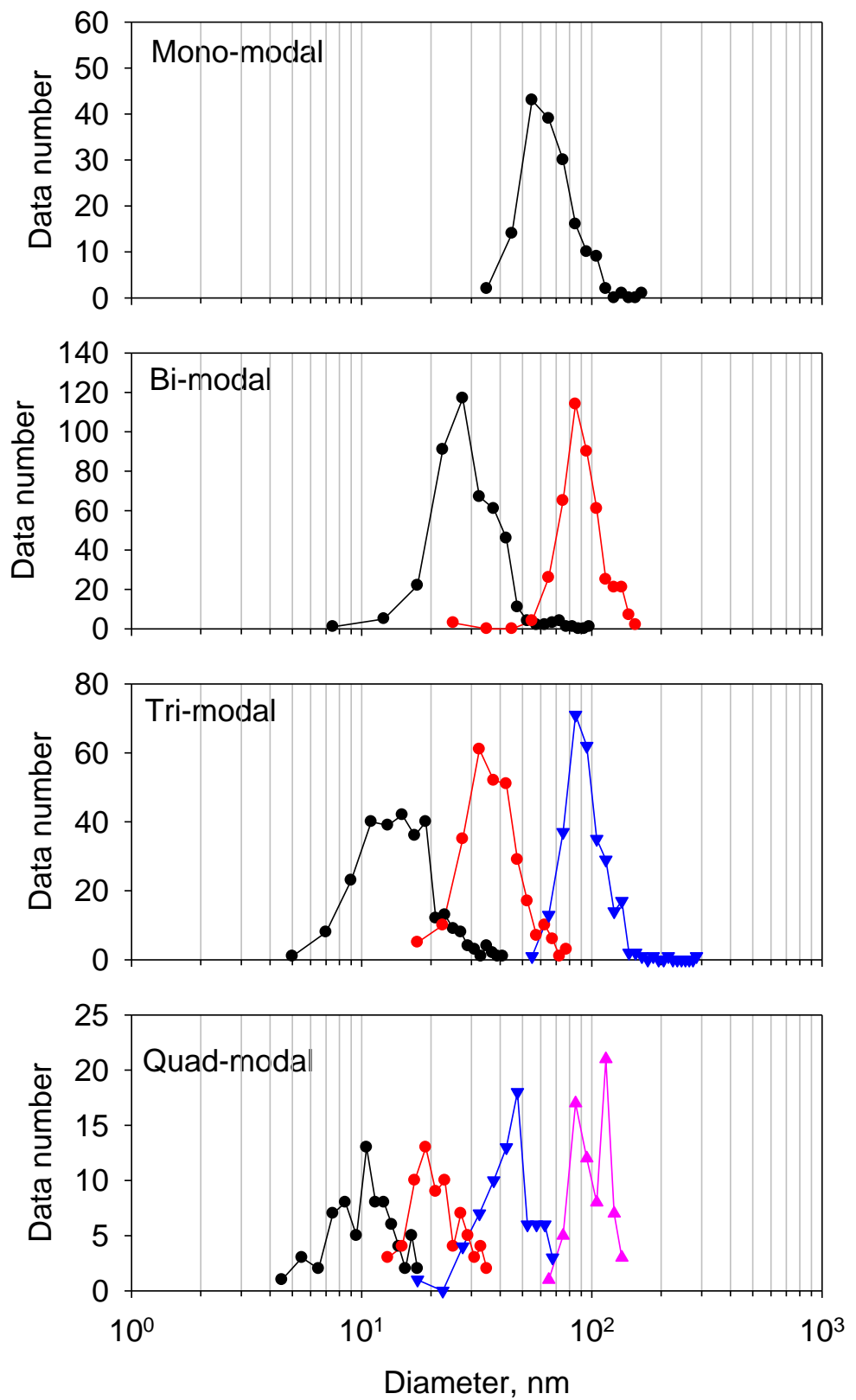
Figure 3: Histogram of modal sizes in each modal structure. Symbols and lines of black, red, blue, and magenta show histograms of 1st, 2nd, 3rd, and 4th modes in each modal structure.
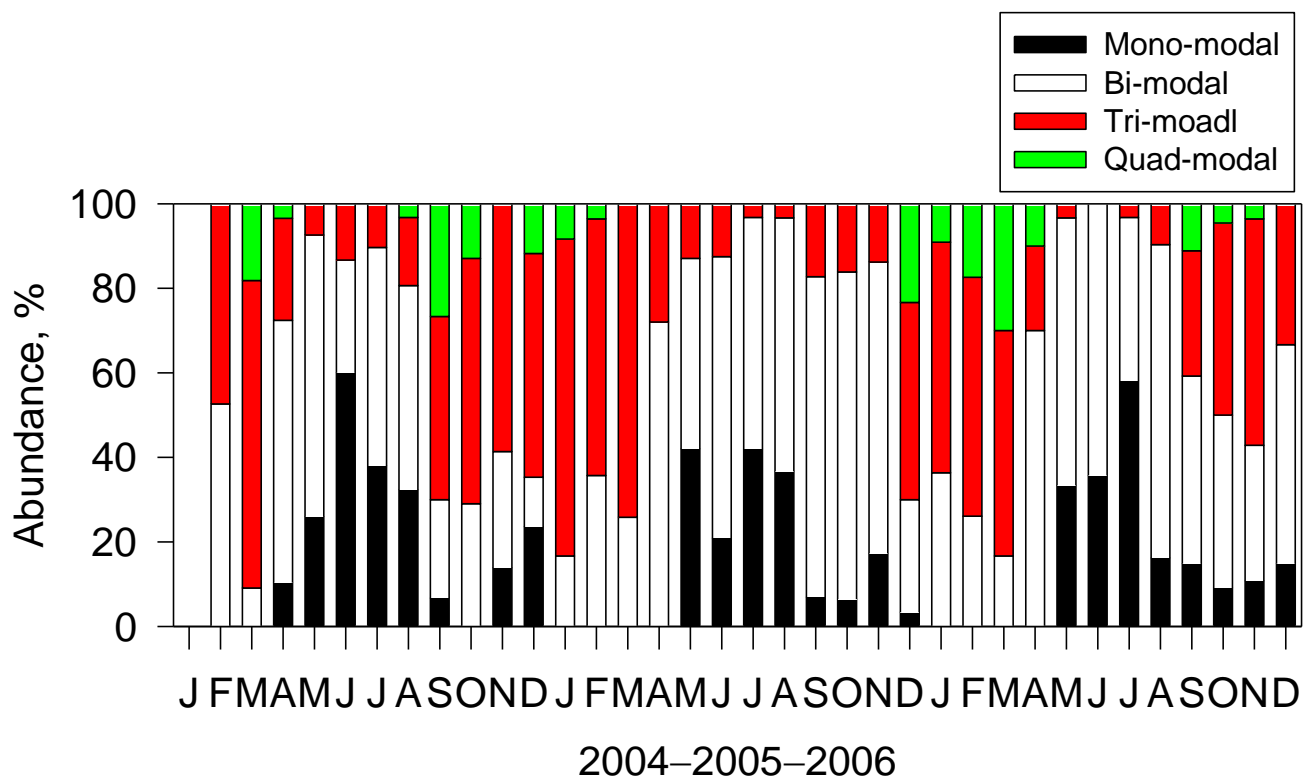
Figure 4: Seasonal feature of abundance of modal structure observed at Syowa Station, Antarctica.

700
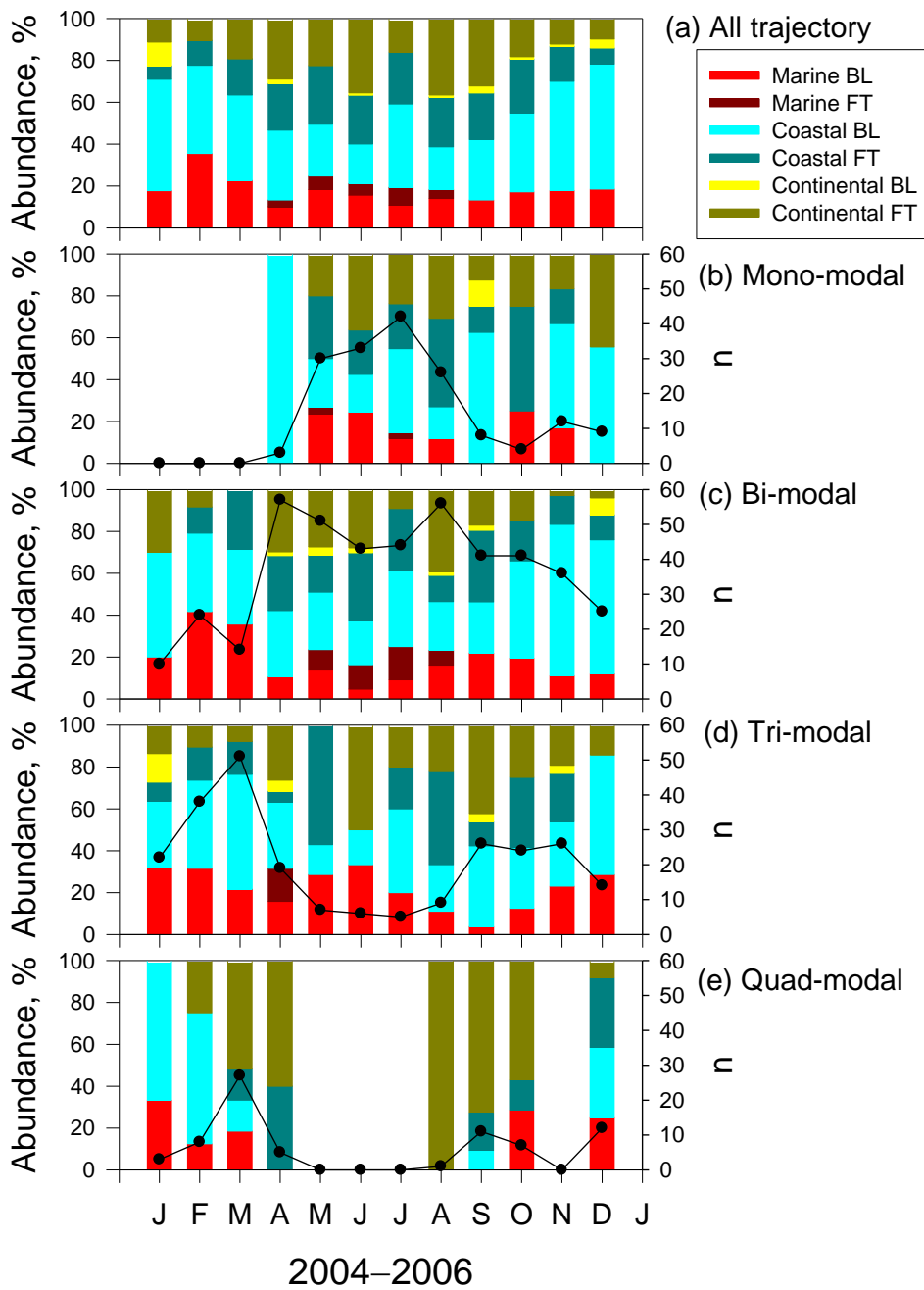
Figure 5: Seasonal feature of air mass origins of (a) all trajectory, (b) mono-modal structure, (c) bi-modal structure, (d) tri-modal structure, and (e) quad-modal structure at Syowa Station, Antarctica. Black line, black circles, and "n" represent the number of the appearance of each modal structure.
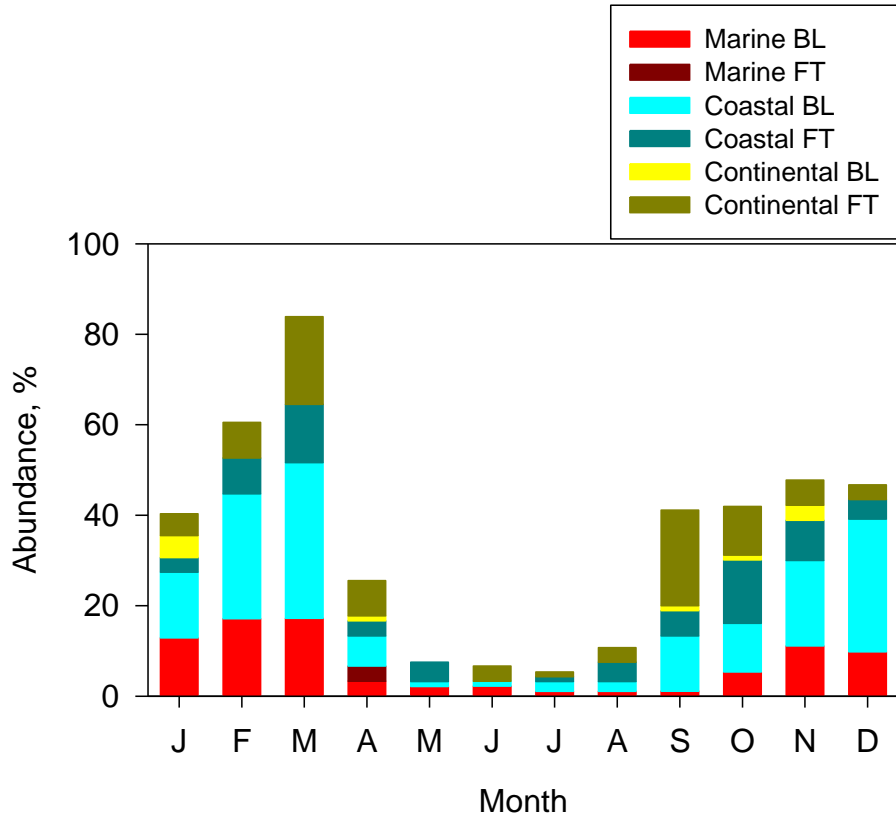
Figure 6: Seasonal feature of abundance of tri- and quad modal structures and air mass origins at Syowa Station, Antarctica in 2004 - 2006.

710
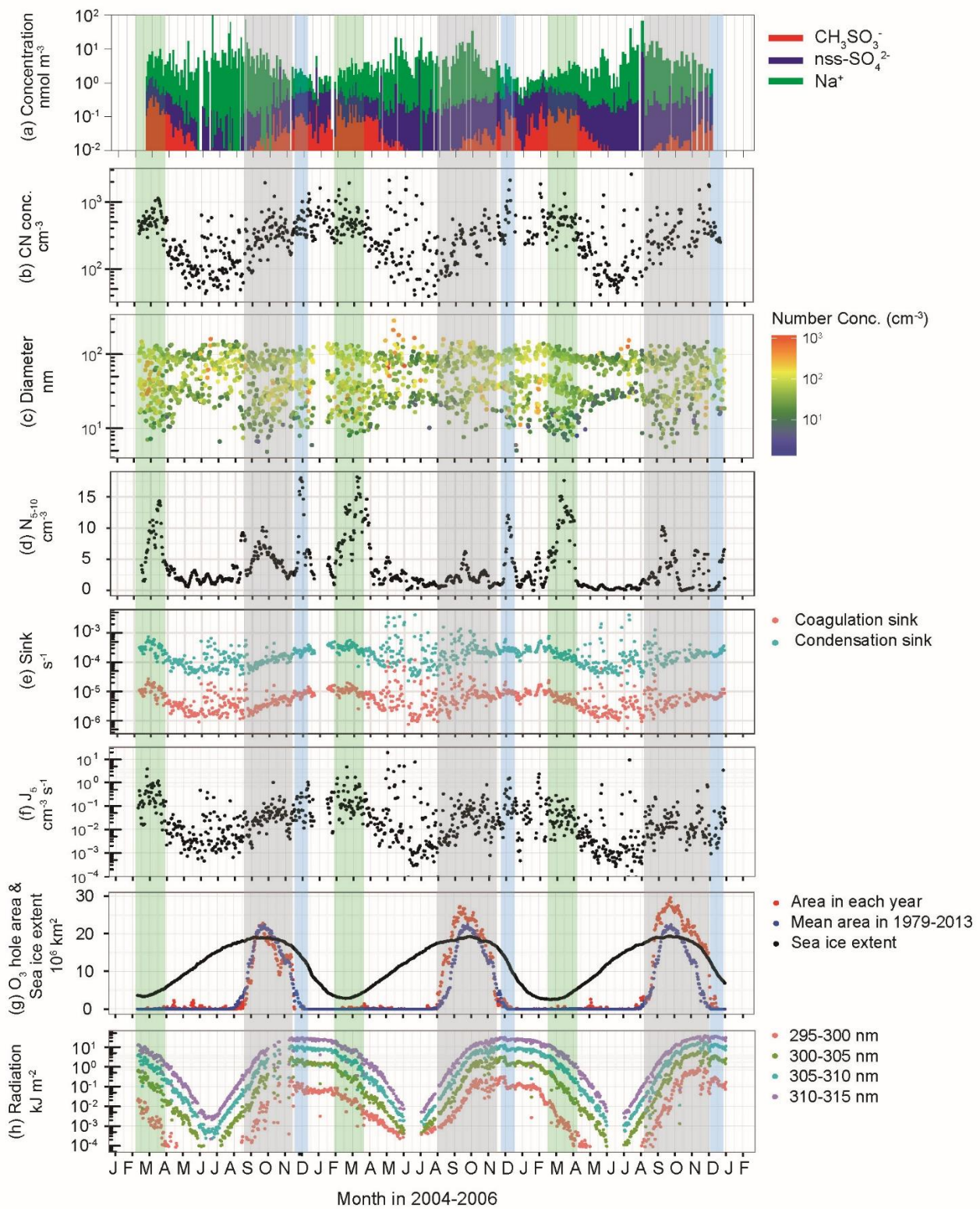
Figure 7: Seasonal variations of (a) the concentrations of $CH_3SO_3^-$, non-sea-salt (nss-) SO_4^{2-} and Na^+ in D_p <200 nm, (b) CN concentrations (D_p >10 nm), (c) modal sizes and number concentrations in each mode, (d) 30-day running mean aerosol number concentrations of fresh nucleation mode (D_p = 5–10 nm), (e) coagulation sink of aerosol particle (D_p = 5nm) and condensation sink, (f) nucleation rate of aerosol particles with Dp = 5 nm (J_5), (g) extent of the Antarctic ozone hole, and (h) UV radiation near surface at Syowa Station, Antarctica during January 2004 – December 2006. Green-shaded, grey-shaded and blue-shaded bands respectively represent periods of minimum of sea-ice extent and high $CH_3SO_3^-$ concentrations, ozone hole appearance and summer solstice. Concentrations of nss-SO_4^{2-} were calculated using Na^+ concentrations and molar ratios in seawater (SO_4^{2-}/ Na^+ = 0.0602; Millero et al., 2008) during November–March and ratios in sea-salts (SO_4^{2-}/Na^+ = 0.01; Hara et al., 2012, 2018) in April–October because the SO_4^{2-}/Na^+ ratio is changed by sea-salt fractionation on sea-ice during April–October (Hara et al., 2012, 2018). The ozone hole extent and sea ice extent data were provided, respectively, by NASA (https://ozonewatch.gsfc.nasa.gov/) and the National Snow & Ice Data Center (https://nsidc.org/data/seaice_index). Daily mean UV data at Syowa Station were monitored by the Japanese Meteorological Agency (http://www.jma.go.jp/jma/index.html) using a Brewer spectrophotometer.
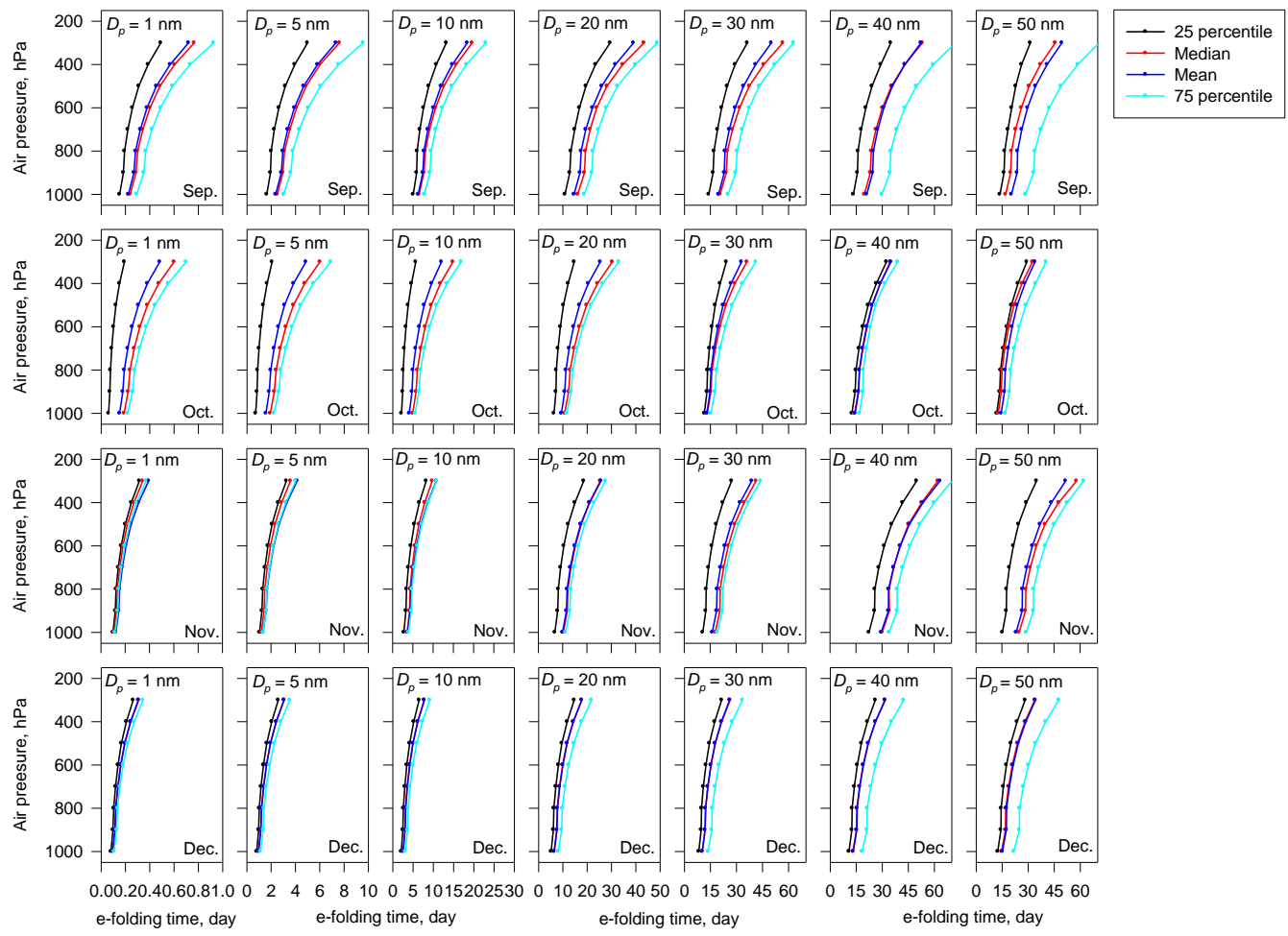
Figure 8: Vertical variations of aerosol e-folding time of coagulation loss in respective sizes in the troposphere over Syowa Station, Antarctica during September – December.

735
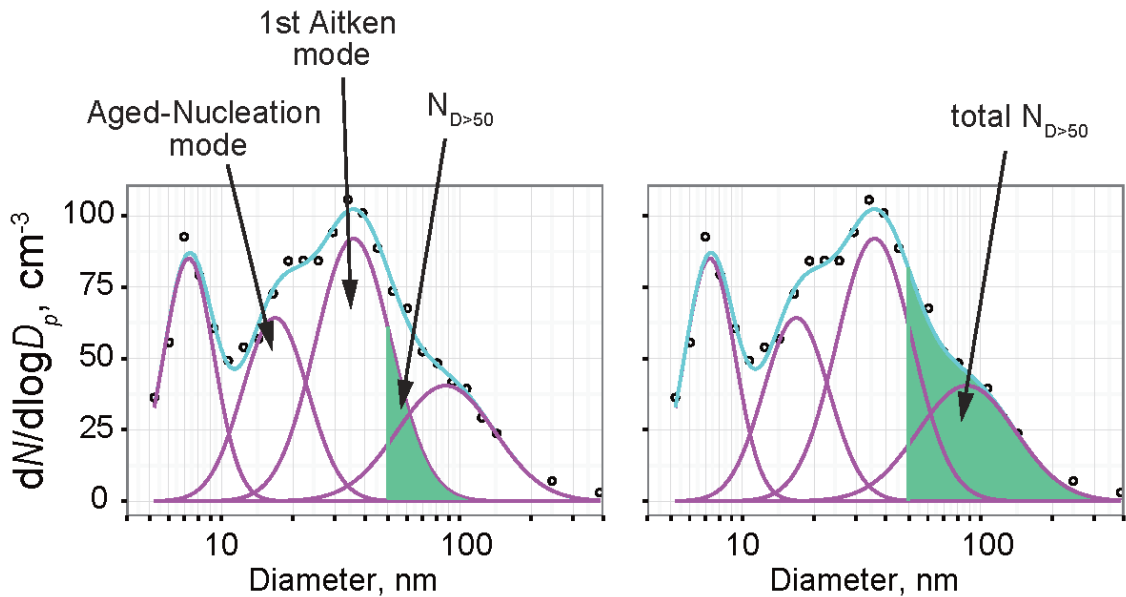
Figure 9: Schematic figure showing procedures used for R$_{CCN}$ estimation. Circles, pink lines, and cyan lines respectively show the data observed using SMPS, the number concentrations in each mode by approximated by lognormal fitting, and total concentrations of each mode. Number concentrations of aerosols with size of D_p>50 nm in aged-nucleation mode and first Aitken mode (N$_{D>50}$) are given as shown for (a). Similarly, the total number concentrations of aerosols with size of D_p>50 nm (total-N$_{D>50}$)

740 **are given as shown for (b).**
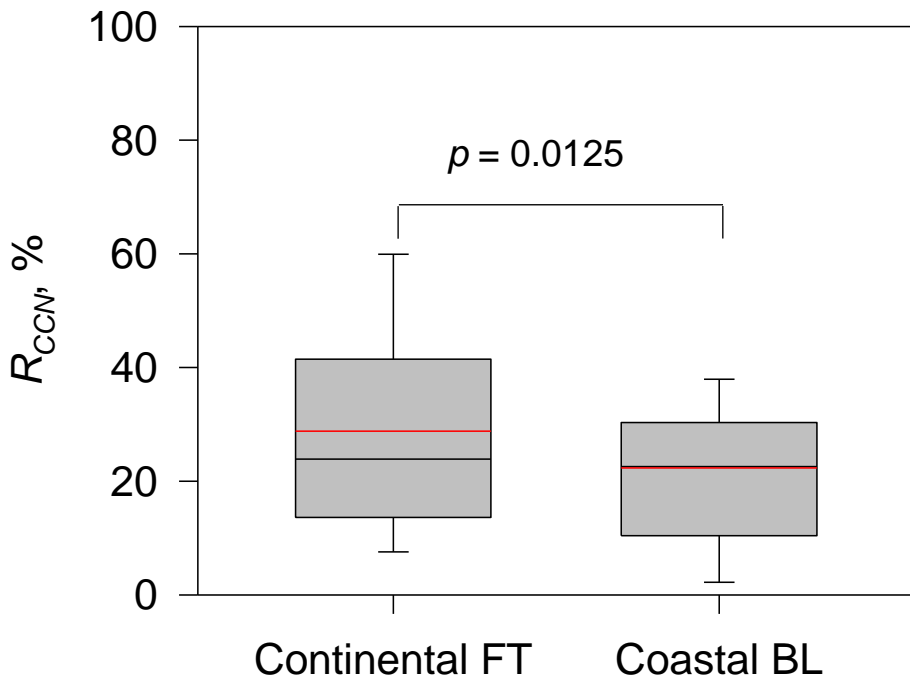
Figure10: Comparison of R$_{CCN}$ **in the continental free troposphere (FT) and those in the coastal boundary layer (BL) during November − January in 2004–2006.** *p* **denote** *p***-value of ANOVA variance test. Degrees of freedom for the ANOVA variance test were 155. Box plots show values of 90, 75, 50 (median), 25, and 10%, denoted respectively by the top bar, top box line, black middle box line, bottom box line, and bottom bar. Red lines show mean values.**
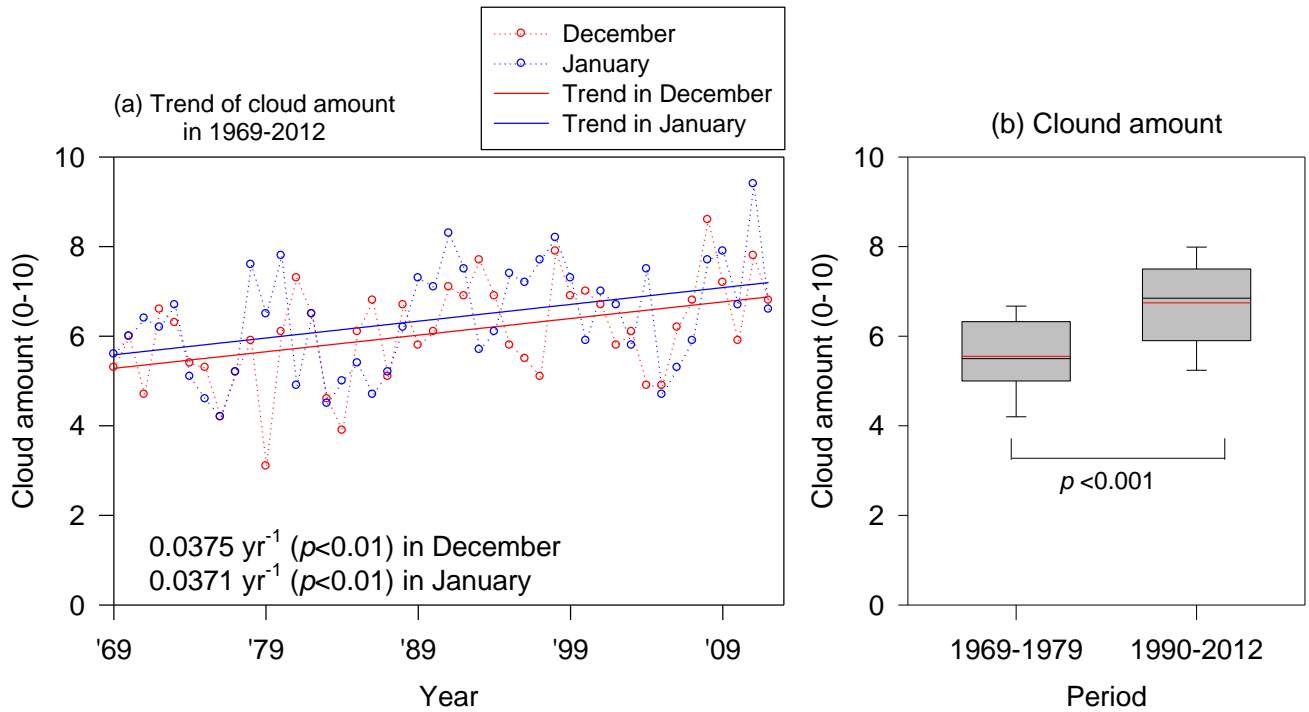
Figure 11(a) Trend of monthly mean cloud amount in 1969–2012 and (b) comparison of cloud amounts in December–January before and after appearance of the Antarctic ozone hole at Syowa Station, Antarctica. *p* **denote** *p*-value of ANOVA variance test. Degrees of freedom for the ANOVA variance test were 66. Because of the extended period of the ozone hole in 1980–1989, cloud amount data in the period were excluded from Fig. 9b. Box plots show values of 90, 75, 50 (median), 25, and 10% denoted respectively by the top bar, top box line, black middle box line, bottom box line, and bottom bar. Red lines show mean values. Cloud amounts were observed based on visual observations by the Japan Meteorological Agency (http://www.jma.go.jp/jma/index.html).
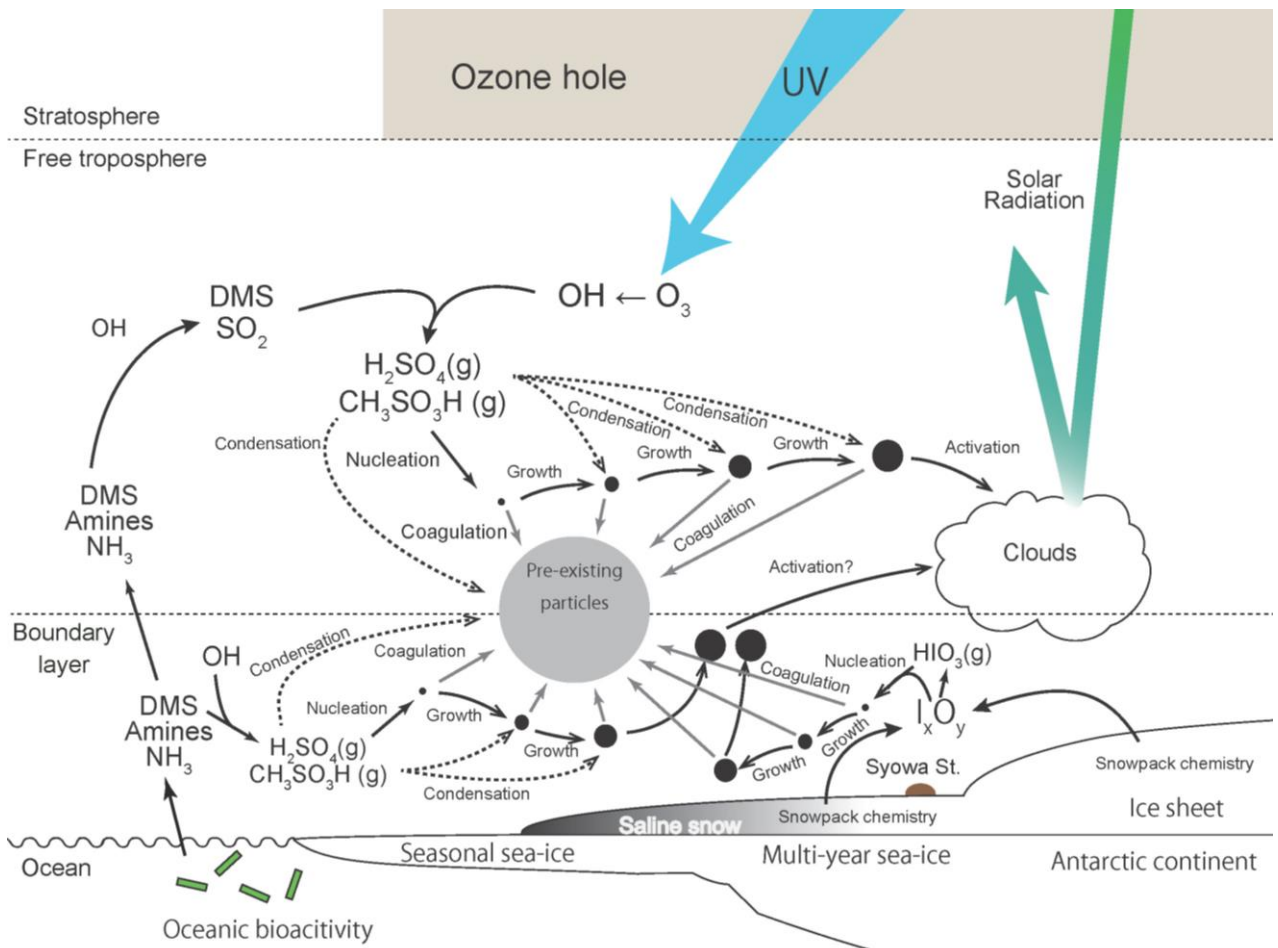
Figure 12: Schematic figure presenting our hypothesis.

760